Extrinsic repair of injured dendrites as a paradigm for regeneration by fusion

Meital Oren-Suissa[1,2], Tamar Gattegno[1], Veronika Kravtsov[1], and Benjamin Podbilewicz[1†]

[1] Department of Biology, Technion- Israel Institute of Technology, Haifa 32000, Israel

[†] Author for correspondence (podbilew@tx.technion.ac.il)

Additional footnotes:

[2] Present address: Howard Hughes Medical Institute, Columbia University, Department of Dept. of Biological Sciences, New York, 10027, USA

Highlights

- New system to study dendritic plasticity, regeneration and degeneration
- Following dendrotomy AFF-1 is activated to bypass the lesion via auto-fusion
- Extracellular AFF-1-vesicles derived from the epidermis fuse severed neurons
- EFF-1 prunes injury-induced ectopic sprouting
- Combined activities of the fusogens EFF-1 and AFF-1 regenerate arbors

Abstract

Injury triggers regeneration of axons and dendrites. Research identified factors required for axonal regeneration outside the CNS, but little is known about regeneration triggered by dendrotomy. To determine how neurons regenerate dendrites following injury we study the *C. elegans* PVD polymodal neurons that display an arborized pattern of repetitive menorah-like structures. We injure dendrites by laser microsurgery, follow their fate and show that broken primary dendrites often regenerate via fusion. We describe how PVD dendrites regenerate and present roles for EFF-1 and AFF-1 glycoproteins in fusion and remodeling of menorahs. Menorahs lose self-avoidance and AFF-1 fuses them, bypassing the injury site. Branch sprouting, EFF-1-mediated pruning, and arbor simplification completes regeneration. When auto-fusion fails the distal arbor degenerates. Surprisingly, AFF-1 acts non-cell autonomously to mediate dendrite fusion. We propose that extracellular vesicles derived from the lateral epidermis fuse severed dendrites in a process reminiscent of enveloped virus-mediated cell fusion without infection.

48

49 ## Introduction

50 Sensory perception relies on networks of neurons that monitor and modify behavior to
51 assure that animals are able to locate food, sense their environment and avoid
52 predators or other threats [1]. This perception depends on the integrity and spatial-
53 coverage of the receptive field [2]. Axonal and dendritic trees play an essential role in
54 processing and transducing information to ultimately evoke the appropriate response
55 of the organism. In the central nervous system (CNS) of adult mammals axon
56 regeneration following injury is limited [3]. Therefore, the regenerative process
57 following axon severing has been the focus of numerous studies [3-5]. It is believed that
58 the main reasons why axons fail to regenerate are a reduction in neuronal growth
59 capacity and inhibitory extrinsic factors. However, the molecular mechanisms of
60 regeneration are not well understood. Recent studies have suggested that modulation
61 of intrinsic neuronal activity by mammalian target of rapamycin (mTOR) and G-
62 protein-coupled receptor (GPCR) signaling promote axon regeneration [4,6]. In parallel
63 there is evidence for a molecular pathway for axonal degeneration that affects
64 regeneration [7]. The molecular mechanisms required for regeneration by regrowth
65 following axonal injury are actively studied and numerous pathways have been
66 identified [3-5,8-12]. In contrast to regeneration by regrowth, a different strategy for
67 axonal regeneration that has been observed in diverse invertebrates is reconnection by
68 fusion of severed axons [13-18].

69 The nematode *C. elegans* is a powerful model to study neuronal regeneration
70 after injury. It has been recently found that injured axons of motor- and
71 mechanosensory-neurons regrow and in some cases fuse after *in vivo* severing using

72 laser surgery [15,16,18-20]. Moreover, screens for genes with roles in axon regrowth
73 identified many genes required for axon regeneration [15,21,22].
74 Compared to axonal regeneration and degeneration pathways, much less is
75 known about dendritic regeneration following injury [23-27]. Recent studies have
76 identified the PVD and FLP neurons as highly branched bilateral neurons in *C.*
77 *elegans,* which display a stereotypic arborization pattern composed of repetitive
78 structural units known as menorahs (**Figures 1A and 1B**)[28-36]. The PVD is highly
79 polarized with a single axon ventral to the cell body and a complex but stereotyped
80 dendritic arbors [32,36] making it an ideal system to study different aspects of the
81 generation, maintenance, regeneration and degeneration of dendritic trees. The PVD
82 neurons are two polymodal nociceptors, responsible for an avoidance response
83 generated after harsh mechanical stimuli to the main body or exposure to cold
84 temperatures [1,37,38]. Animals in which PVD neurons are laser-ablated fail to respond to
85 harsh touch [37]. Recent studies uncovered the degenerin ion channels DEG/ENaC,
86 MEC-10 and DEGT-1 that sense harsh-touch, and the TRPA-1 channels that respond
87 to cold temperatures [34,39]. Moreover, researchers have identified numerous genetic
88 pathways involved in dendritic arborization and maintenance of the PVD structure
89 [32,40-46].
90 The dynamic pathway of PVD arborization revealed an unexpected function of
91 EFF-1 fusogenic protein in sculpting neuronal trees [32]. EFF-1 mediates epithelial and
92 muscle cell-to-cell fusion [47-52], auto cell fusion in the digestive tract [53], axonal fusion
93 following injury [15,17,18,20] and acts in the PVD neurons to trim menorahs [32]. *eff-1*
94 mutants have hyperbranched disorganized menorahs and EFF-1 cell-autonomous
95 expression is sufficient to reduce the number of branches and to rescue disorganized
96 menorahs [32]. EFF-1 controls dendritic plasticity via retraction of excess branches, by

97 fusing branches and by forming loops that restrict further growth [32]. AFF-1, a paralog
98 of EFF-1, mediates fusion of the anchor cell to form the utse/hymen, fuses the lateral
99 epidermal seam cells and merges some embryonic epithelial cells [54]. In addition, AFF-
100 1 is induced by Notch to auto-fuse a myoepithelial toroid [53], and fuses the excretory
101 duct cell to form a single-cell tube [55].

102 Here we studied neuronal plasticity triggered by dendrotomy and determined
103 the fate of complex PVD arbors following laser surgery of dendrites. We found that
104 severed primary dendrites grew towards each other and reconnected via branch
105 fusion. Simultaneously, terminal branches lost self-avoidance and grew towards each
106 other, meeting and fusing at the tips via an AFF-1-mediated process. Ectopic branch
107 growth was identified as a step in the regeneration process required for bypassing the
108 lesion site. Failure of reconnection to the severed dendrites resulted in degeneration of
109 the distal end of the neuron. We discovered pruning of excess branches via EFF-1 that
110 acted to recover the original wild-type arborization pattern in a cell-autonomous
111 process. In contrast, AFF-1 activity during dendritic auto-fusion was derived from the
112 lateral seam cells and not autonomously from the PVD neuron. We propose a model
113 in which AFF-1-vesicles derived from the epidermal seam cells fuse neuronal
114 dendrites from without. Thus, EFF-1 and AFF-1 fusion proteins emerge as new
115 players in neuronal arborization and maintenance of arbor connectivity following
116 injury in *C. elegans*. Our results demonstrate that there is a genetically determined
117 multi-step pathway to repair broken dendrites in which EFF-1 and AFF-1 act on
118 different steps of the pathway. Intrinsic EFF-1 is essential for dendritic pruning after
119 injury and extrinsic AFF-1 is transported in vesicular carriers to mediate dendrite
120 fusion and to bypass injuries.

121

122 ## Results

123 **Dissection of dendritic regeneration in *C. elegans* mechanosensory neurons**

124 The regenerative ability of axons following injury has been previously described in
125 vertebrates and invertebrates [14,56-59]. The morphological and molecular changes that
126 occur following dendritic amputation remain mostly unexplored [23-26,32,60,61]. To study
127 the process of regeneration of the PVD dendrites following amputation we performed
128 dendrotomy of arborized neurites using a femtosecond laser [8,15,16,19]. A successful
129 regeneration was defined as a process in which the severed branch was able to
130 reconnect with its target [62]. Failure to rejoin the two parts of the severed primary
131 dendrite results in degeneration of the distal part and in some cases a complete
132 degeneration without regrowth of the multi-menorah dendritic tree. Temporal analysis
133 of PVD dendrite dynamics following injury revealed several overlapping steps in
134 arbor regeneration (**Figure 1C**). PVD dendrites showed robust regeneration when
135 severed at the L4 stage. We found that severed primary dendrites grew towards each
136 other (**Movies 1 and 2)** and in around 40% of the animals were able to reconnect the
137 distal end to the soma via fusion (**Figure 1D and 1E**).

138 It was shown that following axotomy of the PLM mechanosensory neuron,
139 reconnection of the axon to the distal branch is dependent upon EFF-1, but not AFF-1
140 activity [17,18,20]. In contrast, we found that primary dendrotomies in *eff-1* or *aff-1* single
141 null mutants were repaired and regeneration via primary branch fusion occurred
142 (**Figure 1F**). Due to the sub-viability of *eff-1aff-1* double mutants [54], we were unable
143 to test whether there is redundancy between these genes in primary branch fusion. It is
144 conceivable that there is redundancy in the fusion machinery that fixes broken
145 neurites or that an unidentified fusogen is required for postembryonic primary
146 dendrite auto-fusion after microsurgery. Failure to reconnect following dendrotomy

147 resulted in degeneration of the distal end and took place within 12 hr in about 20% of
148 the operated animals (**Figure 1G**, arrow, **1H** and **Movie 3**). Thus, following primary
149 branch microsurgery the two ends grow towards each other, the tips meet, connect
150 and the integrity of the distal arbors is maintained.

151 **Dendrotomy reveals menorah plasticity and causes loss of self-avoidance**

152 The dendritic architecture of the PVDs is maintained by a contact-dependent self-
153 avoidance mechanism. The tertiary branches withdraw upon contact of a neighboring
154 branch, maintaining the menorah architecture [33,42]. To test whether self-avoidance is
155 maintained after injury, we explored the spatial dynamics of regenerating dendrites.
156 Two hours after injury, we observed tertiary branches from neighboring menorahs
157 that contacted each other and extended far from their initial location, resulting in a
158 structure of overlapping menorahs throughout the neuron (**Figure 1D and 1E**,
159 bracket). Some of these overlaps extended and occurred between menorahs
160 originating from both sides of the lesion (**Figure 1-figure supplement 1 brackets**
161 **and Movies 1 and 2**). These overlapping structures persisted even 48 hr after the
162 injury (**Figure 1-figure supplement 1F**). Dendrotomy at earlier stages, such as the L3
163 stage, showed similar results; animals exhibited loss of avoidance-mechanisms and
164 branch overlap (data not shown). These results suggest that upon injury the avoidance
165 mechanisms are lost, making it more likely that a new connection will form to
166 compensate for the injury.

167 **Menorah-menorah fusion bypasses the severed primary dendrites**

168 We have previously shown that during wild type development PVD and FLP terminal
169 quaternary branches can auto-fuse with one another to maintain menorah structure
170 and to limit further growth [32]. To determine whether fusion of terminal dendrites is
171 part of the regeneration process, we analyzed the overlapping branches after injury

172 and found that most of the reconnections bypassed the injury site through menorah-
173 menorah fusion, resulting in giant menorahs (**Figures 2A-2D, and Figure 2- figure**
174 **supplement 1B,** brackets). To judge the connectivity of the tertiary branches we
175 verified that the distal processes do not degenerate, and analyzed GFP-signal
176 continuity using confocal microscopy and live imaging (**Figure 2D**, **Movies 1, 2 and**
177 **4**). In addition we used a photoactivatable Kaede cytoplasmic reporter expressed in
178 the PVD to demonstrate that the menorahs have fused and therefore have connected to
179 bypass the lesion site (**Figure 2- figure supplement 2**). We found that in animals
180 where menorah-menorah fusion took place the distal fragment did not degenerate,
181 regardless of primary-primary branch reconnection (n=23). Thus, terminal branch
182 auto-fusion acts as a mechanism to bridge the gap between the PVD soma and the
183 distal end to maintain connectivity and avoid degeneration.

184 **Sprouting, pruning, and arbor simplification complete regeneration**

185 We observed that the PVD dendrites appeared highly dynamic after injury, showing
186 ectopic growth of terminal branches. These results suggested that growth is not
187 restricted to a subset of branches, and can occur throughout the neuron, allowing for
188 massive regeneration (**Figures 2C and S1**; asterisks). To verify that growth is
189 stimulated specifically due to the dendrite injury and not because of laser damage, we
190 examined mock-injured animals for PVD morphology changes. We injured animals
191 near the PVDs, at the same focal plane, but without hitting any dendrite. PVD mock-
192 operated animals showed normal growth with no excess sprouting or changes in the
193 PVD morphology (data not shown). These results demonstrate that dendrite severing
194 specifically induced terminal branch reconnection by fusion, ectopic sprouting and
195 regeneration (**Figure 1C**, **Movies 1 and 2**).

196 Interestingly, some of the distal secondary stems were eliminated following
197 the reconnection, leaving just one or two secondary stems per giant menorah (**Figures**
198 **2C and Figure 2- figure supplement 1B**; arrows). These dendritic rearrangements
199 persisted even 48 hr after surgery, leading to simplification of the dendritic trees and
200 leaving mainly giant menorahs. Thus, active elimination of excess branches occurs in
201 order to recreate a pattern resembling wild-type menorahs. Analysis of time-lapse
202 movies showed that excess branches were eliminated, and pruning occurred
203 concomitantly with growth around the injury site (**Figure 2D** and **Movie 4**). Taken
204 together, the PVD dendrites are able to successfully regenerate following dendrotomy,
205 inducing dynamic remodeling by branch growth and elimination (**Figure 1C**).

206 **EFF-1 is essential for pruning excess branches after dendrotomy**

207 The central function of EFF-1 in PVD developmental arborization is in quality control
208 trimming of excess and abnormal branches [32]. To determine whether EFF-1 acts in
209 simplification following injury we amputated primary dendrites in *eff-1* mutants and
210 followed the repair process. We found that *eff-1* mutants maintained hyperbranched
211 and disorganized menorahs and failed to simplify the dendritic tree following injury
212 (**Figure 2E**). These phenotypes suggest that *eff-1* acts in branch retraction and
213 simplification induced by severing of the primary branch. We were not able to
214 determine whether *eff-1* participates in menorah-menorah fusion because the
215 hyperbranched and severely disorganized arbors prevented us from identifying
216 menorah fusion and additional ectopic sprouting (**Figure 2F**). In contrast, both uncut
217 and dendrotomized *eff-1* mutants showed no pruning, demonstrating that *eff-1* is
218 required for branch simplification following dendrotomy. In addition, cell-
219 autonomous expression of EFF-1 in the PVD resulted in excess pruning. Thus, EFF-1

220 acts cell autonomously to simplify excess sprouting following dendrotomy and is
221 sufficient to trim branches and simplify arbors.

222 **AFF-1 is required to bypass cut dendrites via menorah-menorah fusion**

223 Since the *C. elegans* known fusogens, EFF-1 and AFF-1, are essential and sufficient
224 to fuse cells in *C. elegans* and heterologous cells in culture [49,50,54,63,64], we
225 hypothesized that they may be required to regenerate broken neurites by homotypic
226 fusion.

227 Because EFF-1 prunes dendrites by branch retraction we decided to determine
228 a possible role for *aff-1* following dendrotomy, we asked whether menorah-menorah
229 fusion occurs in *aff-1* injured-mutants. We found that while in *aff-1* mutants dendrite
230 development was normal (**Figure 3A**), following dendrotomy most of the
231 reconnections were between the re-growing primary dendrite and its distal fragment,
232 rather than through menorah fusion as in wild-type animals (**Figure 3D**). This
233 observation suggests a fusogenic function for AFF-1 in terminal branch fusion. In *aff-*
234 *1* mutant animals we found some exceptions in which some menorahs overlapped, but
235 we did not observe fusion between menorahs followed by secondary stem
236 degeneration (**Fig. 3D**). In dendrotomized *aff-1* animals failure to rejoin the dendritic
237 trees resulted in degeneration of the distal part of the arbor (**Figs. 3A and 3D**). Thus,
238 while *aff-1* has no apparent role in normal PVD arborization, it is required for
239 terminal branch fusion following dendrotomy.

240 AFF-1-mediated membrane fusion of terminal branches emerges as the main
241 mechanism by which dendritic repair occurs in *C. elegans*. We were not able to detect
242 *aff-1* expression in the PVD neither before nor after dendrotomy. To determine
243 whether AFF-1 acts extrinsically to the PVD to reconnect dendrites we attempted to
244 rescue menorah-menorah fusion in *aff-1* mutant using expression of *grd-10p*::AFF-1

245 in the epidermal seam cells. We found induced recovery of reconnection and reduced
246 degeneration to wild-type levels (**Figure 3B-3D**). In contrast, we found that PVD
247 expressing *des-2p*::AFF-1 was not able to rescue the menorah-menorah fusion failure
248 phenotype (**Figure 3D**). Expression of *dpy-7p::aff-1* from the hypodermis was toxic
249 in *aff-1* homozygous mutants but improved PVD regeneration in heterozygous *aff-1/+*
250 animals, suggesting that non-autonomous expression from the surrounding
251 hypodermis is also sufficient to improve the ability of the PVD to rejoin the branches
252 by fusion (**Figure 3-figure supplement 1**). The non-cell autonomous activity of AFF-
253 1 in PVD regeneration by auto-fusion was unexpected since for cell-cell fusion AFF-1
254 acts homotypically in both fusing plasma membranes [64].

255 **AFF-1-containing extracellular vesicles repair the PVD by fusing with it**

256 To determine AFF-1 expression and localization before and after dendrotomy we
257 imaged AFF-1::GFP in worms expressing mCherry in the PVD. We could not detect
258 AFF-1 in the PVD at any stage during development or following dendrotomy. Instead,
259 AFF-1 is strongly expressed on the plasma membrane, filopodia and internal puncta
260 in the lateral seam cells. This was expected since the seam cells fuse homotypically
261 between the L4 and adult molt via AFF-1-mediated fusion [54]. Using structured
262 illumination microscopy we found extracellular puncta containing AFF-1::GFP that
263 apparently were derived from the seam cells. (**Figure 4A,** arrowheads). Using live
264 spinning disk confocal microscopy we found that the vesicles containing AFF-1::GFP
265 were observed outside the seam cells in control animals that were not dendrotomized
266 (**Figure 4B, Movies 5, 6 and 9**). Following dendrotomy the AFF-1::GFP signal in the
267 seam cells was brighter (**Figure 4C**) and there was a five-fold increase in the mobility
268 and number of extracellular vesicles (**Figure 4D-4F, Movies 7, 8, 10 and 11**). Thus,

269 taken together our results show that AFF-1 regenerates severed PVD dendrites in a
270 surprisingly non-cell autonomous way from the seam cells.
271

272 ## Discussion

273 **AFF-1-extracellular vesicles merge injured neurons from without**

274 Cell-cell fusion from within occurs when a fusogenic protein (e.g. a viral fusion
275 protein following infection) or an endogenous cellular fusion protein (e.g. EFF-1) is
276 expressed intrinsically in cellular compartments, including the plasma membrane.
277 Fusion from without occurs when a viral particle fuses target cells without infecting
278 them [65-67]. Here we discovered an example of fusion from without during neuronal
279 regeneration. We propose that epidermal seam cells shed extracellular vesicles that
280 travel 1000 nm or less to reach the PVD severed dendrites and the menorahs. These
281 vesicles contain AFF-1 and can fuse dendrites from without (**Figure 5**). AFF-1-
282 containing vesicles derived from the lateral epidermal seam cells mediate fusion of
283 severed dendrites and menorah auto-fusion to bypass the injury and to maintain
284 dendritic tree structure and function. Extracellular vesicles (EVs, microvesicles,
285 exosomes and ectosomes) from different sub-cellular and tissue origins have been
286 proposed as vehicles for cell-cell communication during normal physiology,
287 participate in the immune response, control coagulation and promote metastatic
288 cancer [68]. These extracellular vesicles have been shown to exist in bacteria, archea,
289 plants, fungi and animals [69-73]. In *C. elegans* EVs derived from ciliated neurons affect
290 mating behavior and communication between animals [74]. Signaling EVs derived from
291 the sperm activate oogenesis and ovarian muscle contraction [75]. EVs also participate
292 in engulfment of dead cells [76] and morphogenesis of the embryo [77].

293 EVs are probably universal but diverge in size, shape and place of origin.
294 They contain lipid bilayers, transmembrane proteins and nucleic acids. One of the
295 characteristics of these EVs is their ability to fuse to target cells and deliver RNAs,
296 plasmids, toxins and signaling molecules. However, the fusion proteins necessary to
297 deliver and merge the diverse EVs have not been identified and characterized in any
298 system. Mammalian cells transfected with *C. elegans* AFF-1 produce extracellular
299 vesicles that have been biochemically and ultrastructurally characterized [64,78].
300 Moreover, AFF-1-containing vesicles and pseudotyped particles are able to fuse to
301 mammalian cells expressing EFF-1 or AFF-1. Thus, AFF-1 can mediate fusion of
302 extracellular vesicles to cells expressing EFF-1 on the plasma membrane in a tissue
303 culture system [64,78]. Here we provide the initial evidence for a mechanism that can
304 fuse EVs to target neuronal cells in vivo. Surprisingly, these EVs can cause auto-
305 fusion from without mediated by AFF-1 transmembrane fusion protein on their
306 surface. Moreover, these AFF-1-EVs derived from the *C. elegans* lateral epithelia can
307 fuse neurons in vivo, thus directly promoting regeneration (**Figure 5**).

308 **Neurodevelopmental genetic stages in dendrite repair after injury**

309 The primary mechanism of PVD dendritic regeneration can be divided into five
310 stages: (1) reattachment at site of injury, (2) loss of self-avoidance between adjacent
311 menorahs, (3) menorah-menorah fusion to bypass lesions, (4) sprouting of
312 compensatory branches and (5) pruning of excess branches (**Figure 1C**).
313 The interplay between two effector fusogens revealed a genetic pathway that
314 links membrane remodeling during normal development and following neuronal
315 injury. Here we focused on two cellular stages: Extrinsic stage (3) AFF-1-mediated
316 menorah-menorah fusion from without and intrinsic stage (5) EFF-1-mediated
317 trimming of excess branches from within. (**Figures 1C** and **5**).

318 **AFF-1 merges terminal branches to bypass broken dendrites**

319 Axonal fusion after injury is crucial for reestablishing synaptic contacts, to prevent
320 degeneration, and for regaining neurological functionality [62]. Although *eff-1* mutants
321 failed to fuse broken axons [20], *eff-1* mutants succeed to merge injured dendrites. We
322 tested the two known *C. elegans* fusogens, EFF-1 and AFF-1, as well as the EFF-1
323 paralog, C26D10.7 ([50,79] and Oren-Suissa and Podbilewicz, unpublished results). We
324 found that terminal-branch fusion following dendrotomy was significantly reduced in
325 *aff-1* mutants compared to wild-type. However, none of these genes was
326 independently required for primary dendrite fusion following an injury, suggesting
327 either redundancy or that yet another *C. elegans* fusogen awaits identification. Based
328 on these observations, we conclude that *aff-1* is required to heal dendritic wounds,
329 specifically via menorah-menorah fusion.

330 Our data support a model in which *aff-1* and *eff-1* expression is highly
331 regulated in the PVD. Following dendrotomy *eff-1* expression appears to be repressed
332 allowing ectopic sprouting of terminal branches and loss of self-avoidance
333 culminating with AFF-1-mediated menorah-menorah fusion via a surprising non-
334 autonomous mechanism of fusion from without (**Figure 5**).

335 **EFF-1 retracts and simplifies excessive branching following injury**

336 The development of the nervous system includes the formation of many new
337 branches, yet some of them are later eliminated. This process is termed pruning and is
338 crucial for the formation of stable connections. [80-85]. In the central and peripheral
339 nervous systems, axons that are severed from their cell bodies degenerate by the
340 genetically active process of Wallerian degeneration (WD) [7]. WldS mutant mice
341 present slow WD and the persistent axon fragments appear to prevent regeneration by
342 regrowth [7]. In addition, the ubiquitin/proteasome system acts to regulate axon

343 degeneration in Drosophila, in vitro and in mice [86]. Thus, failure to remove axon
344 debris following injury may physically block regeneration by regrowth of severed
345 axons and WD appears to be required for efficient regeneration by regrowth [87].
346 Developmental pruning occurs in *C. elegans* AIM interneurons, and this process is
347 regulated by the helix-turn-helix transcription factor MBR-1 [88] and Wnt-Ror kinase
348 signaling [81]. Here, we demonstrated a novel mechanism of branch pruning following
349 injury. We have previously shown that significant refinement is required to maintain
350 the complex web of dendrites in the final state of perfectly sculpted PVD menorahs [32].
351 This dynamic nature persists following dendrotomy, and many new branches sprout
352 around the injury site to ensure a successful connection will occur. This burst of
353 growth is followed by the elimination of excess branches, and the arbor is simplified
354 to resemble the original tree. This process is normally repressed probably by
355 transcriptional mechanisms. Following injury and a stimulation of ectopic branching,
356 *eff-1* is activated to simplify the arbors and regenerate a normal structure of menorahs.
357 These results suggest that there is conservation of the molecular machinery for neurite
358 refinement, and that the ability to alter existing morphologies is a key component in
359 the development and survival of nervous systems.

360 **Is auto-fusion an alternative pathway to repair severed neurons?**

361 Fusion of severed axons occurs in invertebrates for example in Aplysia [13], crayfish[14]
362 and *C. elegans* [15-18] but rarely in vertebrates [6,89]. Why is this the case and how can our
363 study help us understand this? Invertebrates and vertebrates do have conserved
364 pathways to regenerate injured branches via regrowth [3,4,9,15,90-92]. However, it appears
365 that fusion of broken neurites or bypassing the injured site using fusion instead of
366 rebuilding complex trees is a more energetically economical process. The use of
367 extracellular vesicles could be a useful strategy to stimulate repair of injured branches

368 in the CNS of vertebrates that usually cannot regenerate.

369 **Severed neurites can reconnect by suspending self-repulsion mechanisms**

370 We have found that in *C. elegans* PVD, following dendrotomy there is a transient loss
371 of self-avoidance between the menorahs (tertiary branches) that allows the
372 reconnection by merging the menorahs and bypassing the site of injury, thus
373 maintaining the dendritic trees. This is consistent with studies in leech embryos
374 showing that laser microbeam severing of neurites of mechanosensory neurons result
375 in that the detached branch stopped being avoided by the rest of the cell. This is
376 consistent with a mechanism that controls self-avoidance and that requires physical
377 continuity between the neurites [93]. In *C. elegans* this mechanism appears to involve
378 netrins [42]. In contrast, in zebrafish detached fragments continue to repel the parent
379 arbor [87]. Thus in zebrafish and probably in other vertebrates it is required to have a
380 WD-like mechanism to remove fragments of sensory neurites before the process of
381 regrowth can occur. It would be useful to find ways to induce merging of the severed
382 neurites as occurs in some invertebrates.

383 Spinal cord injuries, experimental axotomies, surgical accidents, and diverse
384 forms of neurodegeneration are all conditions that currently cannot be generally
385 repaired [3,6,58,59,94]. Unveiling the mechanism of intrinsic *eff-1*-mediated dendritic
386 simplification and extrinsic *aff-1*-mediated neuronal auto-fusion from without may
387 pave the way for overcoming neurodegenerative diseases or injuries. The dynamic
388 dendritic plasticity of the PVD neurons and the power of genetics in *C. elegans* along
389 with its amenability for RNAi-based analysis and genome editing will uncover
390 genetic pathways that will enable the study of additional mechanisms involved in
391 PVD arborization during development and following injuries. In *C. elegans* AFF-1-

392 containing vesicles derived from epithelia appear to fuse dendrites emerging as a
393 potential effector that could repair broken neurons in heterologous systems.

394 **Acknowledgements**

395 We thank A. Fire for vectors, M. Krause for *myo-2::gfp,* the *C. elegans* knockout
396 consortium for the *eff-1(ok1021)* deletion allele, M. Heiman and C. Yip for CHB392,
397 C. Smith and D. Miller for NC1841. We also thank A. Sapir, B. Gildor, and J. Grimm
398 for critically reading the manuscript, and E. Oren for MATLAB advice. Supported by
399 grants from Israel Science Foundation, grants 826/08, 443/12 and BIKURA grant
400 1542/07, and the European Research Council advanced grant ELEGANSFUSION
401 268843 to B. P**.** Some strains were provided by the CGC, which is funded by NIH
402 Office of Research Infrastructure Programs (P40 OD010440).

403

404 **Materials and Methods**

405 **Strains and transgenic animals**

406 All nematode strains were maintained according to standard protocols [95,96]. In addition
407 to the wild-type strain N2, the following mutations, transgenes and strains were used:
408 BP601 *aff-1(tm2214)/mIn1[dpy-10(e128) mIs14] II* [54], MF190 *hmIs4[DES-2::GFP,*
409 *pRF4],* BP328 *eff-1(ok1021) II; hmIs4*, BP450 *hyEx30[myo-2::gfp, DES-2::GFP,*
410 *KS],* BP431 *eff-1(hy21) II; hmIs4* [32], NC1841 (*wdIs52, F49H12.4::gfp*; *rwIs1*, *pmec-*
411 *7::*RFP) [33], CHB392 *[hmnEx133(ser-2prom3::kaede)],* kindly provided by Candice
412 Yip and Max Heiman [97]. Germline transformation was performed using standard
413 protocols [98]. The KS bluescript plasmid was used as carrier DNA. Transgenic lines
414 include: BP709 *[hmnIs133 (ser-2prom3::kaede)], BP1014 aff-1/mln1;*
415 *dzIs53[pF49H12.4::mCherry]Is* was created by crossing *aff-1/ mln1*with
416 *pF49H12.4::mCherry* (kindly provided by Salzburg Y.). BP1015 *aff-1/mln1;*

417 *hmnIs133[ser-2prom3::kaede]; hyEx66 [KS , pCFJ90 (myo-2::mcherry), pME4(des-*
418 *2::AFF-1)]*. BP1017 *aff-1/mln1; hmnIs133[ser-2prom3::kaede]; hyEx350[KS*
419 *,pCFJ90 myo-2::mcherry, pTG5 dpy-7p::aff-1],* BP1052 *aff-1/mln1; hmnIs133[ser-*
420 *2prom3::kaede]; hyEx355[KS, pCFJ90 myo-2::mcherry, pTG4 grd-10p::aff-1],*
421 BP1055 *dzIs53[F49H12.4p::mCherry]; hyEx66[pRF4, AFF-1fosmid::GFP, KS],*
422 BP1056 *dzIs53[F49H12.4p::mCherry]; hyEx68[pRF4, AFF-1 fosmid::GFP, KS].*

423 **Molecular Biology**

424 We used RF cloning to insert the *grd-10* promoter upstream to the *aff-1* gene [99], and
425 Gateway cloning [100] to clone *aff-1* into a plasmid containing the *dpy-7* promoter
426 fragment (pDest Dpy7 and pDONR™221). Phusion Hot Start II High-Fidelity DNA
427 polymerase (Thermo Scientific, Waltham, MA) was used to facilitate the cloning
428 process.

429 **Confocal microscopy and live imaging *of C. elegans***

430 Nematodes were mounted on 3% agar pads mixed with 10 mM NaN_3 in M9 buffer.
431 For time-lapse analysis, worms were anesthetized with 0.1% tricaine and 0.01%
432 tetramisol in M9 solution [101-103]. Animals were analyzed by Nomarski optics and
433 fluorescence microscopy, using Zeiss LSM 510 META confocal, the Zeiss LSM 700
434 confocal or Nikon eclipse Ti inverted microscope equipped with Yokogawa CSU-X1
435 spinning disk (Yokogawa, Tokyo, Japan) and a sCMOS (Andor, Belfast, UK) camera.
436 Z-stacks were taken with PlanApochromat 60x oil NA=1.4 objective using the SDC
437 or 63x NA=1.4 objective using the LSM. When using the sCMOS (Andor) camera z-
438 stacks were taken with ~0.35 µm z-step. When the LSM 510 meta was used, z-step
439 was ~0.8 µm. Image acquisition was done using Andor iQ or Metamorph software
440 (Molecular Devices, Sunnyvale, CA) when using the spinning disk confocal (SDC),
441 and Zen software when using the LSM 510 meta microscope or Zeiss LSM 700.

442 Multidimensional data was reconstructed as projections using the ImageJ and
443 Metamorph softwares. Figures were prepared using ImageJ, Adobe Photoshop CS5
444 and Adobe Illustrator CS6.

445 **Quantifying PVD branching phenotypes and statistics**

446 Quantification was done as previously described [32]. Using confocal microscopy, at
447 least five sequential z-series pictures were taken from each worm. Each z-section was
448 analyzed separately. The results from each worm were normalized to a longitudinal
449 length of 100 μm in all relevant experiments. Significant differences between mutants
450 and wild-type were determined by the two-tailed unpaired t-test, the nonparametric
451 Mann-Whitney test or Fischer's exact test. For each group we observed >20 additional
452 animals that were not recorded by z series on the confocal microscope and that
453 showed similar phenotypes.

454 **Laser surgery**

455 Microsurgery was done using the LSM 510 META and a tunable multiphoton
456 Chameleon Ultra Ti-Sapphire laser system (Coherent, Santa Clara, CA), that produces
457 200-fs short pulses with a repetition rate of 113 MHz and 5 nJ energy at a wavelength
458 of 820 nm. 0.5-2 μm^2 selected rectangular ROIs of GFP-labeled PVD neurons were
459 cut and successful surgery was confirmed by visualizing targets immediately after
460 exposure. We evaluated the ability of severed neurons to reconnect by analyzing z-
461 stack images of GFP-labeled branches. Dendrotomy was performed on the primary
462 longitudinal process, and the morphological changes were followed for 2 to 72 hours
463 after the surgery. Imaging before and after surgery was done as described above,
464 using the 488 nm line of the Argon laser of the LSM microscope or using the spinning
465 disk confocal system. After surgery, animals were recovered to an agar plate and
466 remounted 5-72 hours after surgery. Recovered worms were analyzed for

467 regeneration, fusion between processes, and ectopic sprouting. At least 10 individuals
468 were observed for each experiment. For all worms the primary dendrite was injured
469 anterior to cell body. Animals were imaged and a z-stack was collected immediately
470 after injury to confirm a successful injury.

471 **Photoactivation using Kaede**

472 In order to verify that dendrites fuse as response to injury we used the
473 photoconvertible protein Kaede driven by a PVD specific promoter *ser-2prom3* [97]. A
474 PVD primary dendrite of *ser-2prom3::Kaede* expressing animals was dendrotomized,
475 animals were recovered for 23 hours and the dendrite reconnection to its stump was
476 assessed by Kaede photoconversion (Kravtsov et al., in revision). The green Kaede
477 form in the PVD cell body was irreversibly photoconverted to the red Kaede form
478 using a 405 nm laser with the Mosaic system (Andor) on the Nikon eclipse Ti
479 inverted microscope. Following photoconversion of the Kaede in the cell body we
480 followed spreading to the dendritic branches for 1 and 60 min post photoconversion.
481 Red Kaede form, though diluted while spreading through the dendritic tree, can be
482 observed beyond the reconnection site of injury in the distal part of the primary and
483 higher ordered dendritic branches. When the dendrites fail to reconnect or
484 immediately after dendrotomy the photoconverted Kaede did not cross the site of
485 injury, revealing that spreading of red Kaede is a reliable tool to confirm rejoining of
486 severed dendrites.

487

488 ## References

489 1 Goodman, M. B. Sensation is painless. *Trends Neurosci* **26**, 643-645 (2003).
490 2 Hall, D. H. & Treinin, M. How does morphology relate to function in sensory
491 arbors? *Trends Neurosci* **34**, 443-451, doi:S0166-2236(11)00108-1
492 [pii]10.1016/j.tins.2011.07.004 (2011).

493 3 Ruschel, J., Hellal, F., Flynn, K. C., Dupraz, S., Elliott, D. A., Tedeschi, A.,
494 Bates, M., Sliwinski, C., Brook, G., Dobrindt, K., Peitz, M., Brustle, O.,
495 Norenberg, M. D., Blesch, A., Weidner, N., Bunge, M. B., Bixby, J. L. &
496 Bradke, F. Axonal regeneration. Systemic administration of epothilone B
497 promotes axon regeneration after spinal cord injury. *Science* **348**, 347-352,
498 doi:10.1126/science.aaa2958 (2015).
499 4 Park, K. K., Liu, K., Hu, Y., Smith, P. D., Wang, C., Cai, B., Xu, B.,
500 Connolly, L., Kramvis, I., Sahin, M. & He, Z. Promoting axon regeneration in
501 the adult CNS by modulation of the PTEN/mTOR pathway. *Science* **322**, 963-
502 966 (2008).
503 5 Taylor, A. M., Blurton-Jones, M., Rhee, S. W., Cribbs, D. H., Cotman, C. W.
504 & Jeon, N. L. A microfluidic culture platform for CNS axonal injury,
505 regeneration and transport. *Nat Methods* **2**, 599-605, doi:nmeth777
506 [pii]10.1038/nmeth777 (2005).
507 6 Li, S., Yang, C., Zhang, L., Gao, X., Wang, X., Liu, W., Wang, Y., Jiang, S.,
508 Wong, Y. H., Zhang, Y. & Liu, K. Promoting axon regeneration in the adult
509 CNS by modulation of the melanopsin/GPCR signaling. *Proc Natl Acad Sci U*
510 *S A* **113**, 1937-1942, doi:10.1073/pnas.1523645113 (2016).
511 7 Coleman, M. P. & Freeman, M. R. Wallerian degeneration, wld(s), and nmnat.
512 *Annual review of neuroscience* **33**, 245-267, doi:10.1146/annurev-neuro-
513 060909-153248 (2010).
514 8 Wu, Z., Ghosh-Roy, A., Yanik, M. F., Zhang, J. Z., Jin, Y. & Chisholm, A. D.
515 Caenorhabditis elegans neuronal regeneration is influenced by life stage,
516 ephrin signaling, and synaptic branching. *Proc Natl Acad Sci U S A* **104**,
517 15132-15137 (2007).
518 9 Yan, D., Wu, Z., Chisholm, A. D. & Jin, Y. The DLK-1 kinase promotes
519 mRNA stability and local translation in C. elegans synapses and axon
520 regeneration. *Cell* **138**, 1005-1018, doi:S0092-8674(09)00723-5
521 [pii]10.1016/j.cell.2009.06.023 (2009).
522 10 Hammarlund, M. & Jin, Y. Axon regeneration in C. elegans. *Curr Opin*
523 *Neurobiol* **27**, 199-207, doi:10.1016/j.conb.2014.04.001 (2014).
524 11 Edwards, T. J. & Hammarlund, M. Syndecan promotes axon regeneration by
525 stabilizing growth cone migration. *Cell reports* **8**, 272-283,
526 doi:10.1016/j.celrep.2014.06.008 (2014).
527 12 Hammarlund, M., Nix, P., Hauth, L., Jorgensen, E. M. & Bastiani, M. Axon
528 regeneration requires a conserved MAP kinase pathway. *Science* **323**, 802-
529 806, doi:10.1126/science.1165527 (2009).
530 13 Bedi, S. S. & Glanzman, D. L. Axonal rejoining inhibits injury-induced long-
531 term changes in Aplysia sensory neurons in vitro. *J Neurosci* **21**, 9667-9677
532 (2001).
533 14 Hoy, R. R., Bittner, G. D. & Kennedy, D. Regeneration in crustacean
534 motoneurons: evidence for axonal fusion. *Science* **156**, 251-252 (1967).
535 15 Ghosh-Roy, A. & Chisholm, A. D. Caenorhabditis elegans: a new model
536 organism for studies of axon regeneration. *Dev Dyn* **239**, 1460-1464,
537 doi:10.1002/dvdy.22253 (2010).
538 16 Yanik, M. F., Cinar, H., Cinar, H. N., Chisholm, A. D., Jin, Y. & Ben-Yakar,
539 A. Neurosurgery: functional regeneration after laser axotomy. *Nature* **432**, 822
540 (2004).
541 17 Neumann, B., Coakley, S., Giordano-Santini, R., Linton, C., Lee, E. S.,
542 Nakagawa, A., Xue, D. & Hilliard, M. A. EFF-1-mediated regenerative axonal

543 fusion requires components of the apoptotic pathway. *Nature* **517**, 219-222
544 (2015).
545 18 Neumann, B., Nguyen, K. C., Hall, D. H., Ben-Yakar, A. & Hilliard, M. A.
546 Axonal regeneration proceeds through specific axonal fusion in transected C.
547 elegans neurons. *Dev Dyn* **240**, 1365-1372, doi:10.1002/dvdy.22606 (2011).
548 19 Bourgeois, F. & Ben-Yakar, A. Femtosecond laser nanoaxotomy properties
549 and their effect on axonal recovery in C. elegans. *Opt Express* **15**, 8521-8531
550 (2007).
551 20 Ghosh-Roy, A., Wu, Z., Goncharov, A., Jin, Y. & Chisholm, A. D. Calcium
552 and cyclic AMP promote axonal regeneration in Caenorhabditis elegans and
553 require DLK-1 kinase. *J Neurosci* **30**, 3175-3183, doi:30/9/3175
554 [pii]10.1523/JNEUROSCI.5464-09.2010 (2010).
555 21 Nix, P., Hammarlund, M., Hauth, L., Lachnit, M., Jorgensen, E. M. &
556 Bastiani, M. Axon regeneration genes identified by RNAi screening in C.
557 elegans. *J Neurosci* **34**, 629-645, doi:10.1523/JNEUROSCI.3859-13.2014
558 (2014).
559 22 Gabel, C. V., Antoine, F., Chuang, C. F., Samuel, A. D. & Chang, C. Distinct
560 cellular and molecular mechanisms mediate initial axon development and
561 adult-stage axon regeneration in C. elegans. *Development* **135**, 1129-1136
562 (2008).
563 23 Standler, N. A. & Bernstein, J. J. Degeneration and regeneration of
564 motoneuron dendrites after ventral root crush: computer reconstruction of
565 dendritic fields. *Experimental neurology* **75**, 600-615 (1982).
566 24 Song, Y., Ori-McKenney, K. M., Zheng, Y., Han, C., Jan, L. Y. & Jan, Y. N.
567 Regeneration of Drosophila sensory neuron axons and dendrites is regulated
568 by the Akt pathway involving Pten and microRNA bantam. *Genes Dev* **26**,
569 1612-1625, doi:10.1101/gad.193243.112 (2012).
570 25 Stone, M. C., Albertson, R. M., Chen, L. & Rolls, M. M. Dendrite injury
571 triggers DLK-independent regeneration. *Cell reports* **6**, 247-253,
572 doi:10.1016/j.celrep.2013.12.022 (2014).
573 26 Stone, M. C., Nguyen, M. M., Tao, J., Allender, D. L. & Rolls, M. M. Global
574 up-regulation of microtubule dynamics and polarity reversal during
575 regeneration of an axon from a dendrite. *Mol Biol Cell* **21**, 767-777,
576 doi:10.1091/mbc.E09-11-0967 (2010).
577 27 Hall, G. F. & Cohen, M. J. Dendritic amputation redistributes sprouting
578 evoked by axotomy in lamprey central neurons. *J Neurosci* **8**, 3598-3606
579 (1988).
580 28 White, J. G., Southgate, E., Thomson, J. N. & Brenner, S. The structure of the
581 nervous system of Caenorhabditis elegans. *Philos. Trans. R. Soc. Lond. B*
582 *Biol. Sci* **314**, 1-340 (1986).
583 29 Halevi, S., McKay, J., Palfreyman, M., Yassin, L., Eshel, M., Jorgensen, E. &
584 Treinin, M. The C. elegans ric-3 gene is required for maturation of nicotinic
585 acetylcholine receptors. *Embo J* **21**, 1012-1020 (2002).
586 30 Tsalik, E. L., Niacaris, T., Wenick, A. S., Pau, K., Avery, L. & Hobert, O.
587 LIM homeobox gene-dependent expression of biogenic amine receptors in
588 restricted regions of the C. elegans nervous system. *Dev Biol* **263**, 81-102
589 (2003).
590 31 Yassin, L., Gillo, B., Kahan, T., Halevi, S., Eshel, M. & Treinin, M.
591 Characterization of the deg-3/des-2 receptor: a nicotinic acetylcholine receptor

592 that mutates to cause neuronal degeneration. *Mol Cell Neurosci* **17**, 589-599
593 (2001).
594 32 Oren-Suissa, M., Hall, D., Treinin, M., Shemer, G. & Podbilewicz, B. The
595 Fusogen EFF-1 Controls Sculpting of Mechanosensory Dendrites. *Science*
596 **328**, 1285-1288, doi:10.1126/science.1189095 (2010).
597 33 Smith, C. J., Watson, J. D., Spencer, W. C., O'Brien, T., Cha, B., Albeg, A.,
598 Treinin, M. & Miller, D. M., 3rd. Time-lapse imaging and cell-specific
599 expression profiling reveal dynamic branching and molecular determinants of
600 a multi-dendritic nociceptor in C. elegans. *Dev Biol* **345**, 18-33, doi:S0012-
601 1606(10)00805-5 [pii]10.1016/j.ydbio.2010.05.502 (2010).
602 34 Albeg, A., Smith, C., Chatzigeorgiou, M., Feitelson, D. G., Hall, D. H.,
603 Schafer, W. R., Miller, D. M., 3rd & Treinin, M. C. elegans multi-dendritic
604 sensory neurons: Morphology and function. *Mol Cell Neurosci* **46**, 308-317,
605 doi:S1044-7431(10)00246-0 [pii]10.1016/j.mcn.2010.10.001 (2011).
606 35 Pujadas, L., Gruart, A., Bosch, C., Delgado, L., Teixeira, C. M., Rossi, D., de
607 Lecea, L., Martinez, A., Delgado-Garcia, J. M. & Soriano, E. Reelin regulates
608 postnatal neurogenesis and enhances spine hypertrophy and long-term
609 potentiation. *J Neurosci* **30**, 4636-4649, doi:30/13/4636
610 [pii]10.1523/JNEUROSCI.5284-09.2010 (2010).
611 36 Maniar, T. A., Kaplan, M., Wang, G. J., Shen, K., Wei, L., Shaw, J. E.,
612 Koushika, S. P. & Bargmann, C. I. UNC-33 (CRMP) and ankyrin organize
613 microtubules and localize kinesin to polarize axon-dendrite sorting. *Nat*
614 *Neurosci* **15**, 48-56, doi:10.1038/nn.2970 (2012).
615 37 Way, J. C. & Chalfie, M. The mec-3 gene of Caenorhabditis elegans requires
616 its own product for maintained expression and is expressed in three neuronal
617 cell types. *Genes Dev* **3**, 1823-1833 (1989).
618 38 Chatzigeorgiou, M., Yoo, S., Watson, J. D., Lee, W. H., Spencer, W. C.,
619 Kindt, K. S., Hwang, S. W., Miller, D. M., 3rd, Treinin, M., Driscoll, M. &
620 Schafer, W. R. Specific roles for DEG/ENaC and TRP channels in touch and
621 thermosensation in C. elegans nociceptors. *Nature neuroscience* **13**, 861-868,
622 doi:10.1038/nn.2581 (2010).
623 39 Chatzigeorgiou, M. & Schafer, W. R. Lateral facilitation between primary
624 mechanosensory neurons controls nose touch perception in C. elegans. *Neuron*
625 **70**, 299-309, doi:10.1016/j.neuron.2011.02.046 (2011).
626 40 Liang, X., Dong, X., Moerman, D. G., Shen, K. & Wang, X. Sarcomeres
627 Pattern Proprioceptive Sensory Dendritic Endings through UNC-52/Perlecan
628 in C. elegans. *Dev Cell* **33**, 388-400, doi:10.1016/j.devcel.2015.03.010 (2015).
629 41 Dong, X., Liu, O. W., Howell, A. S. & Shen, K. An extracellular adhesion
630 molecule complex patterns dendritic branching and morphogenesis. *Cell* **155**,
631 296-307, doi:10.1016/j.cell.2013.08.059 (2013).
632 42 Smith, C. J., Watson, J. D., VanHoven, M. K., Colon-Ramos, D. A. & Miller,
633 D. M., 3rd. Netrin (UNC-6) mediates dendritic self-avoidance. *Nat Neurosci*
634 **15**, 731-737, doi:10.1038/nn.3065 (2012).
635 43 Aguirre-Chen, C., Bulow, H. E. & Kaprielian, Z. C. elegans bicd-1, homolog
636 of the Drosophila dynein accessory factor Bicaudal D, regulates the branching
637 of PVD sensory neuron dendrites. *Development* **138**, 507-518,
638 doi:10.1242/dev.060939 (2011).
639 44 Salzberg, Y., Diaz-Balzac, C. A., Ramirez-Suarez, N. J., Attreed, M., Tecle,
640 E., Desbois, M., Kaprielian, Z. & Bulow, H. E. Skin-Derived Cues Control

641 Arborization of Sensory Dendrites in Caenorhabditis elegans. *Cell* **155**, 308-
642 320, doi:10.1016/j.cell.2013.08.058 (2013).
643 45 Taylor, C. A., Yan, J., Howell, A. S., Dong, X. & Shen, K. RAB-10 Regulates
644 Dendritic Branching by Balancing Dendritic Transport. *PLoS Genet* **11**,
645 e1005695, doi:10.1371/journal.pgen.1005695 (2015).
646 46 Dong, X., Chiu, H., Park, Y. J., Zou, W., Zou, Y., Ozkan, E., Chang, C. &
647 Shen, K. Precise regulation of the guidance receptor DMA-1 by KPC-1/Furin
648 instructs dendritic branching decisions. *eLife* **5**, doi:10.7554/eLife.11008
649 (2016).
650 47 Smurova, K. & Podbilewicz, B. RAB-5- and DYNAMIN-1-Mediated
651 Endocytosis of EFF-1 Fusogen Controls Cell-Cell Fusion. *Cell reports* **14**,
652 1517-1527, doi:10.1016/j.celrep.2016.01.027 (2016).
653 48 Podbilewicz, B. Virus and Cell Fusion Mechanisms. *Annual Review of Cell*
654 *and Developmental Biology* **30**, 111-139 (2014).
655 49 Shemer, G., Suissa, M., Kolotuev, I., Nguyen, K. C. Q., Hall, D. H. &
656 Podbilewicz, B. EFF-1 is sufficient to initiate and execute tissue-specific cell
657 fusion in *C. elegans*. *Curr Biol* **14**, 1587-1591 (2004).
658 50 Mohler, W. A., Shemer, G., del Campo, J., Valansi, C., Opoku-Serebuoh, E.,
659 Scranton, V., Assaf, N., White, J. G. & Podbilewicz, B. The type I membrane
660 protein EFF-1 is essential for developmental cell fusion in *C. elegans*. *Dev*
661 *Cell* **2**, 355-362 (2002).
662 51 Shinn-Thomas, J. H., Del Campo, J. J., Wang, J. & Mohler, W. A. The EFF-
663 1A Cytoplasmic Domain Influences Hypodermal Cell Fusions in C. elegans
664 But Is Not Dependent on 14-3-3 Proteins. *PLoS One* **11**, e0146874,
665 doi:10.1371/journal.pone.0146874 (2016).
666 52 Shinn-Thomas, J. H. & Mohler, W. A. New insights into the mechanisms and
667 roles of cell-cell fusion. *Int Rev Cell Mol Biol* **289**, 149-209,
668 doi:10.1016/B978-0-12-386039-2.00005-5 (2011).
669 53 Rasmussen, J. P., English, K., Tenlen, J. R. & Priess, J. R. Notch signaling and
670 morphogenesis of single-cell tubes in the C. elegans digestive tract. *Dev Cell*
671 **14**, 559-569 (2008).
672 54 Sapir, A., Choi, J., Leikina, E., Avinoam, O., Valansi, C., Chernomordik, L.
673 V., Newman, A. P. & Podbilewicz, B. AFF-1, a FOS-1-Regulated Fusogen,
674 Mediates Fusion of the Anchor Cell in C. elegans. *Dev Cell* **12**, 683-698
675 (2007).
676 55 Stone, C. E., Hall, D. H. & Sundaram, M. V. Lipocalin signaling controls
677 unicellular tube development in the Caenorhabditis elegans excretory system.
678 *Dev Biol* **329**, 201-211, doi:10.1016/j.ydbio.2009.02.030 (2009).
679 56 Bradbury, E. J., Moon, L. D., Popat, R. J., King, V. R., Bennett, G. S., Patel,
680 P. N., Fawcett, J. W. & McMahon, S. B. Chondroitinase ABC promotes
681 functional recovery after spinal cord injury. *Nature* **416**, 636-640 (2002).
682 57 Cajal, S. R. *Histología del sistema nervioso del hombre y de los vertebrados*.
683 2007 edn, Vol. 1 (Ministerio de Sanidad y Consumo, 1899).
684 58 Fernandez-Gonzalez, A., La Spada, A. R., Treadaway, J., Higdon, J. C.,
685 Harris, B. S., Sidman, R. L., Morgan, J. I. & Zuo, J. Purkinje cell degeneration
686 (pcd) phenotypes caused by mutations in the axotomy-induced gene, Nna1.
687 *Science* **295**, 1904-1906 (2002).
688 59 Devor, M. Neuroplasticity in the rearrangement of olfactory tract fibers after
689 neonatal transection in hamsters. *The Journal of comparative neurology* **166**,
690 49-72 (1976).

691 60 Oren-Suissa, M. & Podbilewicz, B. Evolution of programmed cell fusion:
692 Common mechanisms and distinct functions. *Developmental Dynamics* **239**,
693 1515-1528, doi:10.1002/dvdy.22284 (2010).
694 61 Nawabi, H., Zukor, K. & He, Z. No simpler than mammals: axon and dendrite
695 regeneration in Drosophila. *Genes Dev* **26**, 1509-1514,
696 doi:10.1101/gad.198150.112 (2012).
697 62 Hilliard, M. A. Axonal degeneration and regeneration: a mechanistic tug-of-
698 war. *J Neurochem* **108**, 23-32, doi:10.1111/j.1471-4159.2008.05754.x (2009).
699 63 Podbilewicz, B., Leikina, E., Sapir, A., Valansi, C., Suissa, M., Shemer, G. &
700 Chernomordik, L. V. The C. elegans developmental fusogen EFF-1 mediates
701 homotypic fusion in heterologous cells and in vivo. *Dev Cell* **11**, 471-481
702 (2006).
703 64 Avinoam, O., Fridman, K., Valansi, C., Abutbul, I., Zeev-Ben-Mordehai, T.,
704 Maurer, U. E., Sapir, A., Danino, D., Gruenewald, K., White, J. M. &
705 Podbilewicz, B. Conserved Eukaryotic Fusogens Can Fuse Viral Envelopes to
706 Cells. *Science* **332**, 589-592, doi:10.1126/science.1202333 (2011).
707 65 Clavel, F. & Charneau, P. Fusion from without directed by human
708 immunodeficiency virus particles. *J Virol* **68**, 1179-1185 (1994).
709 66 Bratt, M. A. & Gallaher, W. R. Preliminary analysis of the requirements for
710 fusion from within and fusion from without by Newcastle disease virus. *Proc*
711 *Natl Acad Sci U S A* **64**, 536-543 (1969).
712 67 White, J., Matlin, K. & Helenius, A. Cell fusion by Semliki Forest, influenza,
713 and vesicular stomatitis viruses. *J Cell Biol* **89**, 674-679 (1981).
714 68 Tkach, M. & Thery, C. Communication by Extracellular Vesicles: Where We
715 Are and Where We Need to Go. *Cell* **164**, 1226-1232,
716 doi:10.1016/j.cell.2016.01.043 (2016).
717 69 Miyado, K., Yoshida, K., Yamagata, K., Sakakibara, K., Okabe, M., Wang,
718 X., Miyamoto, K., Akutsu, H., Kondo, T., Takahashi, Y., Ban, T., Ito, C.,
719 Toshimori, K., Nakamura, A., Ito, M., Miyado, M., Mekada, E. & Umezawa,
720 A. The fusing ability of sperm is bestowed by CD9-containing vesicles
721 released from eggs in mice. *Proc Natl Acad Sci U S A* **105**, 12921-12926
722 (2008).
723 70 Kwon, S. H., Liu, K. D. & Mostov, K. E. Intercellular Transfer of GPRC5B
724 via Exosomes Drives HGF-Mediated Outward Growth. *Curr Biol* **24**, 199-204,
725 doi:10.1016/j.cub.2013.12.010 (2014).
726 71 Liegeois, S., Benedetto, A., Garnier, J. M., Schwab, Y. & Labouesse, M. The
727 V0-ATPase mediates apical secretion of exosomes containing Hedgehog-
728 related proteins in Caenorhabditis elegans. *J Cell Biol* **173**, 949-961,
729 doi:10.1083/jcb.200511072 (2006).
730 72 Beveridge, T. J. Structures of gram-negative cell walls and their derived
731 membrane vesicles. *J Bacteriol* **181**, 4725-4733 (1999).
732 73 Hyenne, V., Apaydin, A., Rodriguez, D., Spiegelhalter, C., Hoff-Yoessle, S.,
733 Diem, M., Tak, S., Lefebvre, O., Schwab, Y., Goetz, J. G. & Labouesse, M.
734 RAL-1 controls multivesicular body biogenesis and exosome secretion. *J Cell*
735 *Biol* **211**, 27-37, doi:10.1083/jcb.201504136 (2015).
736 74 Wang, J., Silva, M., Haas, L. A., Morsci, N. S., Nguyen, K. C., Hall, D. H. &
737 Barr, M. M. C. elegans ciliated sensory neurons release extracellular vesicles
738 that function in animal communication. *Curr Biol* **24**, 519-525,
739 doi:10.1016/j.cub.2014.01.002 (2014).

740 75 Kosinski, M., McDonald, K., Schwartz, J., Yamamoto, I. & Greenstein, D. C.
741 elegans sperm bud vesicles to deliver a meiotic maturation signal to distant
742 oocytes. *Development* **132**, 3357-3369, doi:10.1242/dev.01916 (2005).
743 76 Mapes, J., Chen, Y. Z., Kim, A., Mitani, S., Kang, B. H. & Xue, D. CED-1,
744 CED-7, and TTR-52 regulate surface phosphatidylserine expression on
745 apoptotic and phagocytic cells. *Curr Biol* **22**, 1267-1275,
746 doi:10.1016/j.cub.2012.05.052 (2012).
747 77 Wehman, A. M., Poggioli, C., Schweinsberg, P., Grant, B. D. & Nance, J. The
748 P4-ATPase TAT-5 inhibits the budding of extracellular vesicles in C. elegans
749 embryos. *Curr Biol* **21**, 1951-1959, doi:10.1016/j.cub.2011.10.040 (2011).
750 78 Fridman, K. *Ultrastructure and function of AFF-1 and EFF-1 in membrane*
751 *remodeling* MSc thesis, Technion - Israel Institute of Technology, (2012).
752 79 Avinoam, O. & Podbilewicz, B. Eukaryotic cell-cell fusion families. *Curr Top*
753 *Membr* **68**, 209-234, doi:B978-0-12-385891-7.00009-X [pii]10.1016/B978-0-
754 12-385891-7.00009-X (2011).
755 80 Jorgensen, E. M. & Rankin, C. in *C. elegans II* (eds D. L. Riddle, T.
756 Blumenthal, B. J. Meyer, & J. R. Priess) (1997).
757 81 Hayashi, Y., Hirotsu, T., Iwata, R., Kage-Nakadai, E., Kunitomo, H., Ishihara,
758 T., Iino, Y. & Kubo, T. A trophic role for Wnt-Ror kinase signaling during
759 developmental pruning in Caenorhabditis elegans. *Nat Neurosci* **12**, 981-987,
760 doi:10.1038/nn.2347 (2009).
761 82 Tessier, C. R. & Broadie, K. Drosophila fragile X mental retardation protein
762 developmentally regulates activity-dependent axon pruning. *Development* **135**,
763 1547-1557 (2008).
764 83 Singh, K. K., Park, K. J., Hong, E. J., Kramer, B. M., Greenberg, M. E.,
765 Kaplan, D. R. & Miller, F. D. Developmental axon pruning mediated by
766 BDNF-p75NTR-dependent axon degeneration. *Nat Neurosci* **11**, 649-658
767 (2008).
768 84 Schuldiner, O., Berdnik, D., Levy, J. M., Wu, J. S., Luginbuhl, D., Gontang,
769 A. C. & Luo, L. piggyBac-based mosaic screen identifies a postmitotic
770 function for cohesin in regulating developmental axon pruning. *Dev Cell* **14**,
771 227-238 (2008).
772 85 Helton, T. D., Otsuka, T., Lee, M. C., Mu, Y. & Ehlers, M. D. Pruning and
773 loss of excitatory synapses by the parkin ubiquitin ligase. *Proc Natl Acad Sci*
774 *U S A* **105**, 19492-19497 (2008).
775 86 Zhai, Q., Wang, J., Kim, A., Liu, Q., Watts, R., Hoopfer, E., Mitchison, T.,
776 Luo, L. & He, Z. Involvement of the ubiquitin-proteasome system in the early
777 stages of wallerian degeneration. *Neuron* **39**, 217-225 (2003).
778 87 Martin, S. M., O'Brien, G. S., Portera-Cailliau, C. & Sagasti, A. Wallerian
779 degeneration of zebrafish trigeminal axons in the skin is required for
780 regeneration and developmental pruning. *Development* **137**, 3985-3994,
781 doi:10.1242/dev.053611 (2010).
782 88 Kage, E., Hayashi, Y., Takeuchi, H., Hirotsu, T., Kunitomo, H., Inoue, T.,
783 Arai, H., Iino, Y. & Kubo, T. MBR-1, a novel helix-turn-helix transcription
784 factor, is required for pruning excessive neurites in Caenorhabditis elegans.
785 *Curr Biol* **15**, 1554-1559, doi:10.1016/j.cub.2005.07.057 (2005).
786 89 Paltsyn, A., Komissarova, S., Dubrovin, I. & Kubatiev, A. Increased cell
787 fusion in cerebral cortex may contribute to poststroke regeneration. *Stroke*
788 *research and treatment* **2013**, 869327, doi:10.1155/2013/869327 (2013).

90 Yaniv, S. P., Issman-Zecharya, N., Oren-Suissa, M., Podbilewicz, B. & Schuldiner, O. Axon Regrowth during Development and Regeneration Following Injury Share Molecular Mechanisms. *Curr Biol* **22**, 1774-1782, doi:10.1016/j.cub.2012.07.044 (2012).

91 Bradke, F., Fawcett, J. W. & Spira, M. E. Assembly of a new growth cone after axotomy: the precursor to axon regeneration. *Nat Rev Neurosci* **13**, 183-193, doi:10.1038/nrn3176 (2012).

92 Mar, F. M., Bonni, A. & Sousa, M. M. Cell intrinsic control of axon regeneration. *EMBO reports* **15**, 254-263, doi:10.1002/embr.201337723 (2014).

93 Wang, H. & Macagno, E. R. A detached branch stops being recognized as self by other branches of a neuron. *Journal of neurobiology* **35**, 53-64 (1998).

94 Moritz, C. T., Perlmutter, S. I. & Fetz, E. E. Direct control of paralysed muscles by cortical neurons. *Nature* **456**, 639-642 (2008).

95 Brenner, S. The genetics of *Caenorhabditis elegans*. *Genetics* **77**, 71-94 (1974).

96 Sulston, J. & Hodgkin, J. in *The Nematode Caenorhabditis elegans* (ed W.B. Wood) 587-606 (Cold Spring Harbor Laboratory, 1988).

97 Yip, Z. C. & Heiman, M. G. Duplication of a Single Neuron in C. elegans Reveals a Pathway for Dendrite Tiling by Mutual Repulsion. *Cell reports*, doi:10.1016/j.celrep.2016.05.003 (2016).

98 Mello, C. & Fire, A. in *Methods in Cell Biology. Caenorhabditis elegans: Model Biological Analysis of an Organism* Vol. 48 (eds H F Epstein & D C Shakes) 451-482 (Academic Press, 1995).

99 Bond, S. R. & Naus, C. C. RF-Cloning.org: an online tool for the design of restriction-free cloning projects. *Nucleic Acids Res* **40**, W209-213, doi:10.1093/nar/gks396 (2012).

100 Petersen, L. K. & Stowers, R. S. A Gateway MultiSite recombination cloning toolkit. *PLoS One* **6**, e24531, doi:10.1371/journal.pone.0024531 (2011).

101 McCarter, J., Bartlett, B., Dang, T. & Schedl, T. On the control of oocyte meiotic maturation and ovulation in Caenorhabditis elegans. *Dev Biol* **205**, 111-128 (1999).

102 McCarter, J., Bartlett, B., Dang, T. & Schedl, T. Soma-germ cell interactions in Caenorhabditis elegans: multiple events of hermaphrodite germline development require the somatic sheath and spermathecal lineages. *Dev Biol* **181**, 121-143 (1997).

103 Kirby, C., Kusch, M. & Kemphues, K. Mutations in the *par* genes of *Caenorhabditis elegans* affect cytoplasmic reorganization during the first cell cycle. *Dev. Biol.* **142**, 203-215 (1990).

829 **Figures**

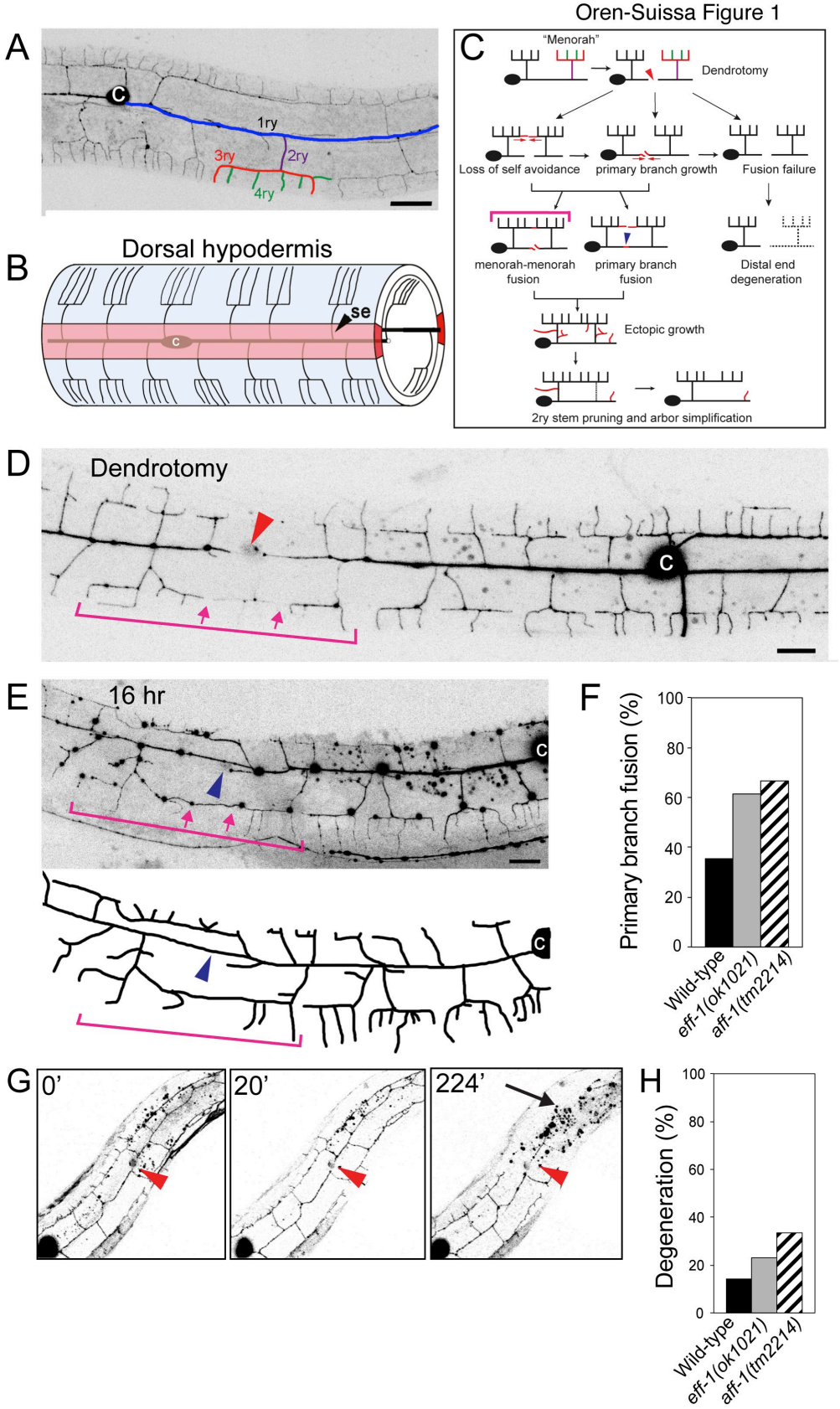

830
831

832 **Figure 1.**
833
834 **Dendrite regeneration of multibranched PVD neurons following laser**
835 **microsurgery in *C. elegans***
836
837 **(A)** A wild-type animal expressing *DES-2::GFP*, illustrating the PVD neuron
838 elaborate branching pattern (inverted image). Branches of one menorah are numbered
839 primary to quaternary (1ry to 4ry), and color-coded: blue, purple, red, and green,
840 respectively [32], c= cell body.
841
842 **(B)** Schematic model of hypodermal cells and PVD menorahs in a young adult, left
843 view. The wild-type PVDs grow between the hypodermis (outer cylinder, light blue)
844 and the basement membrane of the hypodermis (not shown), extending processes that
845 branch out to form the menorah structures. In light red is the left hypodermal seam
846 syncytium. Modified from [32], se= seam cells, c= cell body.
847
848 **(C)** Cartoon summarizing the different stages in PVD regeneration following injury.
849 Two-photon dendrotomy (see Materials and methods) of the primary process (red
850 arrowhead) leads to dynamic changes in the PVD arbor: loss of branch self-avoidance
851 and growth is followed by primary branch fusion (blue arrowhead), menorah-menorah
852 fusion (pink bracket), or both. There is an additional phase of dynamic growth and
853 pruning, leading to arbor refinement. When the branches fail to fuse, the distal end
854 undergoes degeneration.
855
856 **(D-E)** Primary and menorah-menorah fusion following dendrotomy. L4 animal just
857 after surgery (**D**) and 16 hr post-surgery (**E**). Red arrowhead marks the site of
858 dendrotomy. Blue arrowhead marks reconnection site of dendrotomy.
859
860 **(E)** The severed distal and proximal ends of the primary branch reconnected (blue
861 arrowhead). Distal and proximal menorahs fused to form an additional connection
862 between the soma and distal end (Pink arrows and bracket).
863
864 **(F)** Percentage of primary branch fusion during regeneration in wild type (n=14), *eff-*
865 *1(ok1021)* (n=13) and *aff-1(tm2214)* (n=12) dendrotomized animals.
866
867 **(G)** Live imaging of an injured young-adult animal in which reconnection was
868 unsuccessful, and degeneration of the distal arbor occurred. Time after injury is
869 indicated in minutes. Red arrowhead– site of injury. Arrow– degenerating arbor.
870 Images are taken from **Movie 3**. Posterior is up and dorsal is left. Scale bars represent
871 20 μm in (A) and 10 μm in (D-E).
872
873 **(H)** Percentage of animals with degenerating distal end following dendrotomy in wild
874 type, *eff-1(ok1021)* and *aff-1(tm2214)* animals.
875
876

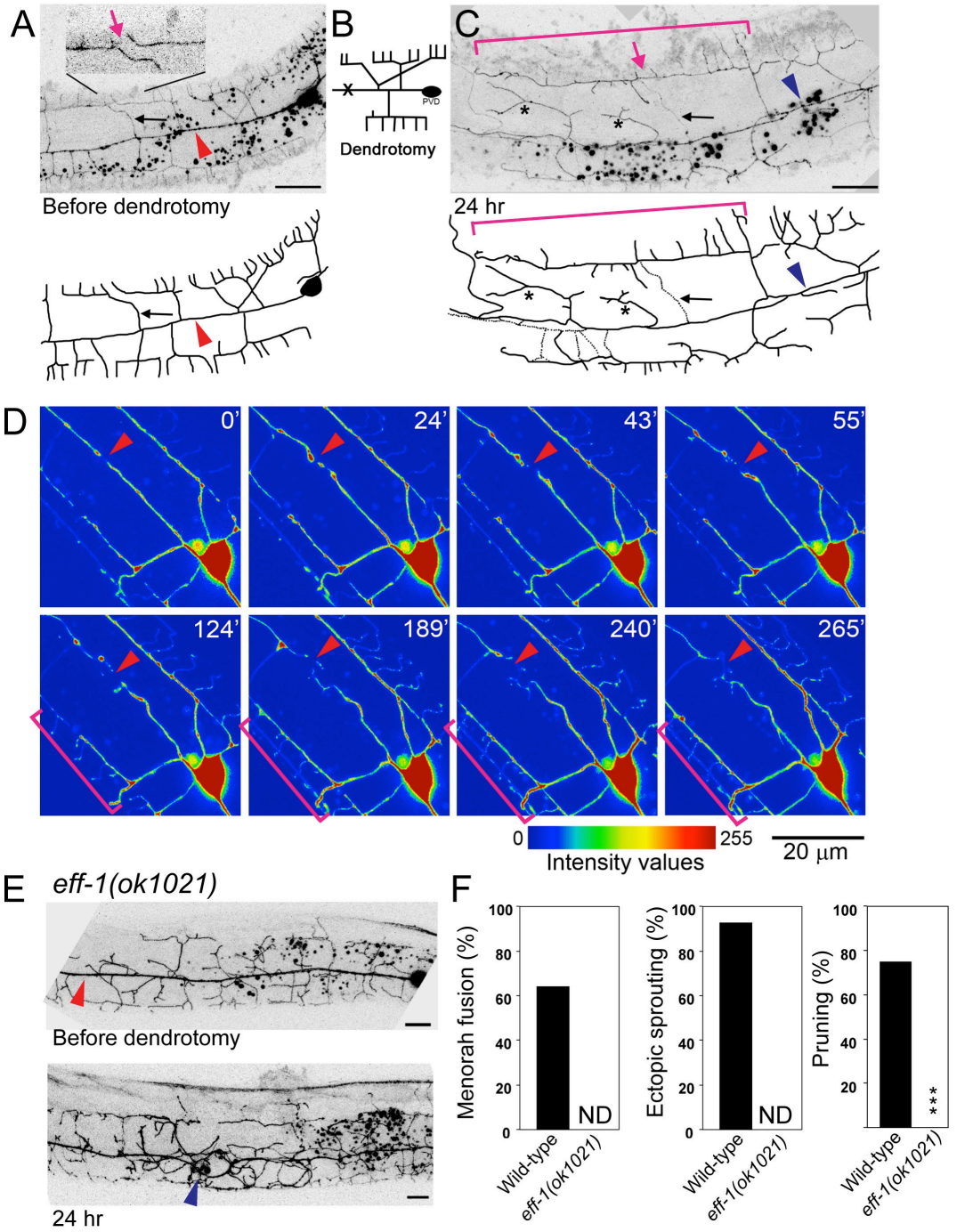
A
B
C
PVD
Dendrotomy
Before dendrotomy
24 hr
D
0'
24'
43'
55'
124'
189'
240'
265'
0
255
Intensity values
20 µm
E
eff-1(ok1021)
Before dendrotomy
24 hr
F
Menorah fusion (%)
Ectopic sprouting (%)
Pruning (%)
100
80
60
40
20
0
ND
ND
***
Wild-type
eff-1(ok1021)

879 **Figure 2.**
880
881 **The dynamic pathway of PVD regeneration after injury**
882
883 **(A-C)** Dendrotomy of an L4 animal resulted in menorah-menorah fusion.
884
885 **(A)** Just prior to the injury separate menorahs can be seen (pink arrow in inset). Red
886 arrowhead points to the lesion site.
887
888 **(B)** Schematic showing the site of injury (marked with an X).
889
890 **(C)** Formation of giant menorahs (pink bracket) and ectopic sprouting (asterisks)
891 within 24 hr. Pink arrow points to the site of loss of self-avoidance. Blue arrowhead
892 points to the site of 1ry-1ry fusion. Pruning of secondary branches also occurs (black
893 arrow, dotted lines, also marked in (**A**)).
894
895 **(D)** Intensity values view of images from a time-lapse movie of injured L4 wild-type
896 worm (**Movie 4**). Time after injury is shown at the upper right corner in minutes.
897 Arrowheads point to injury site and pruning of branches. Brackets mark two
898 menorahs from distal and proximal ends bypassing the break and contacting one
899 another.
900
901 **(E)** *eff-1* animal before and 24 hr after dendrotomy. There is a successful reconnection
902 of the severed primary branch (arrowhead) and pruning failure (the arbor does not
903 undergo simplification). Scale bars represent 10 μm.
904
905 **(F)** Dendrotomy-induced phenotypes in *eff-1(ok1021)* animals. Menorah-menorah
906 fusion, percentage of animals that contained fused giant menorahs; ectopic sprouting,
907 fraction of animals showing growth of additional processes; pruning, percentage of
908 animals in which PVD underwent branch refinement after fusion. In *eff-1(ok1021)*
909 mutants there is excess branching and disorganized branch structure [32], thus we could
910 not determine (ND) whether menorah-menorah connections and ectopic sprouting
911 occurred. ***$P<0.001$, Fisher's exact test. n values: 14, 13 animals for wild-type and
912 *eff-1(ok1021),* respectively.
913

Oren-Suissa Figure 3

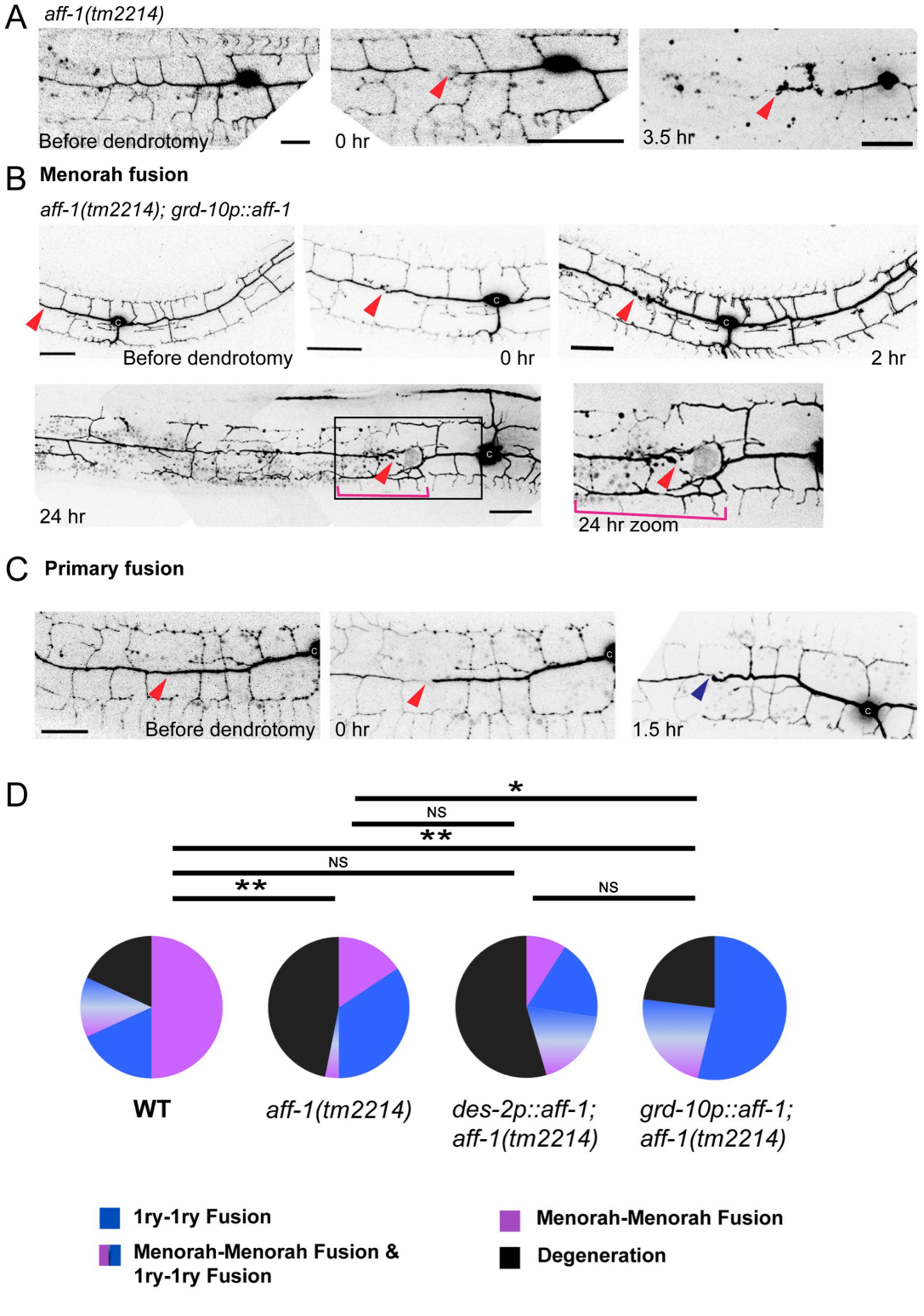

916 **Figure 3.**

917 ***aff-1* dendritic reconnection patterns are rescued cell non-autonomously**

918 **(A)** Dendrite regeneration following PVD nanosurgery in *aff-1(tm2214)* mutant
919 animal. PVD is shown before and after nanosurgery (t=0 and 3.5 hr). In non-injured
920 *aff-1* mutant animals PVD branching pattern is unaffected. After injury, fusion does
921 not occur and the distal processes undergo degeneration (t=3.5 hr).
922
923 **(B)** Dendrite regeneration following PVD nanosurgery in *aff-1(tm2214); grd-10p::aff-*
924 *1* animals. PVD is shown before and after nanosurgery (t=0, 2, and 24 hr). PVD
925 reconnection occurred through fused menorahs (pink bracket). Red arrowhead marks
926 site of injury. Primary branches did not fuse (red arrowhead).
927
928 **(C)** Dendrite regeneration following PVD nanosurgery in *aff-1(tm2214); grd-*
929 *10p::aff-1* animals. PVD is shown before and after nanosurgery (t=0 and 1.5 hr). PVD
930 reconnection occurred through primary fusion (blue arrowhead).
931
932 **(D)** PVD post-injury outcomes displayed in color coded pie graphs as Magenta–
933 Menorah-Menorah fusion, Blue– primary-primary fusion, Magenta and Blue–
934 Menorah-Menorah fusion and primary-primary fusion, Black– degeneration. Wild
935 type n=22, *aff-1(tm2214)* n=32, *aff-1(tm2214);des-2p::aff*-n=11, *aff-1(tm2214); grd-*
936 *10p::aff-1* n=13. ** $P<0.01$; * $P<0.05$; NS $P>0.05$. Dendrotomy site – red arrowhead,
937 fused menorah – pink bracket, primary fusion – blue arrowhead. Scale bars represent
938 20 µm. Statistics was calculated using the Freeman-Halton extension of the Fisher
939 exact probability test for a two-rows by four-columns contingency table,
940 http://vassarstats.net/fisher2x4.html.
941

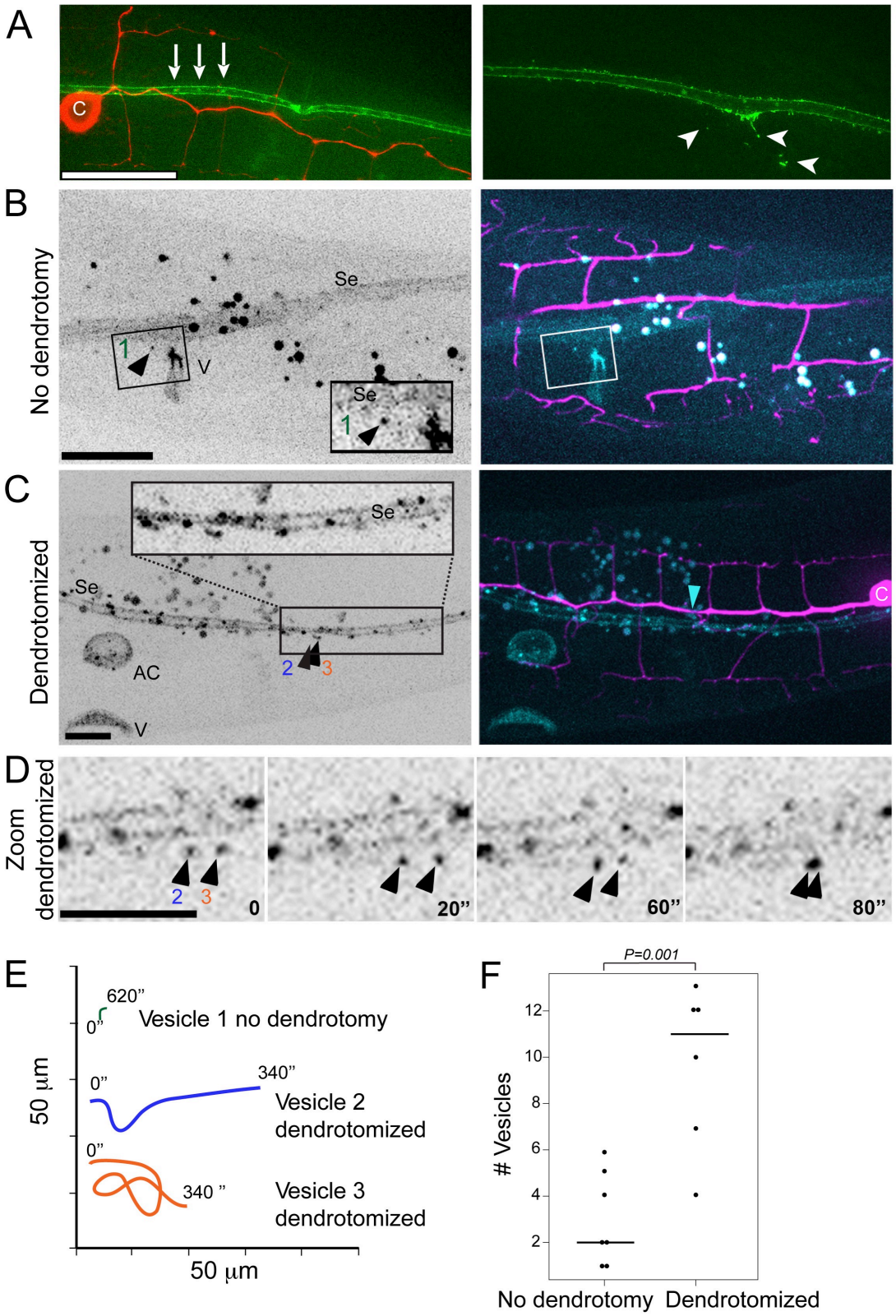
A
C
B
No dendrotomy
Se
1
V
Se
1
C
Dendrotomized
Se
Se
AC
2
3
V
C
D
Zoom dendrotomized
2
3
0
20”
60”
80”
E
50 µm
620”
0”
Vesicle 1 no dendrotomy
0”
340”
Vesicle 2 dendrotomized
0”
340 ”
Vesicle 3 dendrotomized
50 µm
F
P=0.001
# Vesicles
12
10
8
6
4
2
No dendrotomy
Dendrotomized

944 **Figure 4.**
945
946 **AFF-1 protein dynamics during PVD regeneration**
947
948 **(A)** Superresolution structured illumination microscopy (SIM) image of aligned *AFF-*
949 *1::GFP* (green) vesicles in the seam cells (left, white arrows) and *AFF-1::GFP*
950 extracellular vesicles derived from the seam cells (right, white arrowheads) in intact
951 wild type animals. c, cell body. PVD is labeled in red.
952
953 **(B)** Spinning disk confocal images of *AFF-1::GFP* expression inside and outside the
954 seam cells (Se), and in the vulva (V) of an intact L4 animal (left). *AFF-1::GFP* (cyan)
955 expression in the seam cells and in vesicles near the seam cells is shown in a two
956 channels merged image (right; PVD in magenta; **Movie 5**). Inset shows magnification
957 of a single *AFF-1::GFP* vesicle near the seam cells (left, black arrowhead, numbered
958 1; **Movie 6**).
959
960 **(C)** *AFF-1::GFP* expression inside and outside the seam cells (Se), in the anchor cell
961 (AC) and in the vulva (V) of a reconnected PVD L4 animal (left) is shown 2 hr post-
962 dendrotomy in a spinning disk confocal image. *AFF-1::GFP* is expressed in vesicles
963 inside and outside of the seam cells, in the anchor cell (AC) and in VulA ring (see
964 **Movie 7)**. Inset shows magnification of area with multiple vesicles, two are labeled
965 (2,3) and shown in panels **(D-E).**
966
967 **(D)** Two *AFF-1::GFP* vesicles, numbered 2 and 3, are moving near the seam cells in
968 a PVD-dendrotomized animal. Four time points are shown (0, 20, 60 and 80 sec;
969 **Movie 8**).
970
971 **(E)** Vesicles dynamics (1, 2 and 3) is demonstrated in a color-coded graph during 340
972 seconds for vesicles 2 and 3 and 620 seconds for vesicle number 1. The plot illustrates
973 vast differences between *AFF-1::GFP* vesicles movements in animals with an intact
974 PVD versus *AFF-1::GFP* vesicles in PVD dendrotomized animals (**Movies 6 and 8)**.
975
976 **(F)** Dot Plot of the number of *AFF-1::GFP* vesicles outside *aff-1* expressing organs in
977 animals with intact PVD versus in animals with dendrotomized PVD. The graph
978 demonstrates statistical significant difference between the mean number of *aff-*
979 *1::GFP* vesicles outside *aff-1* expressing organs such as seam cells, vulva, anchor cell
980 and the uterus. P=0.001, statistics was calculated using the nonparametric Mann-
981 Whitney test.

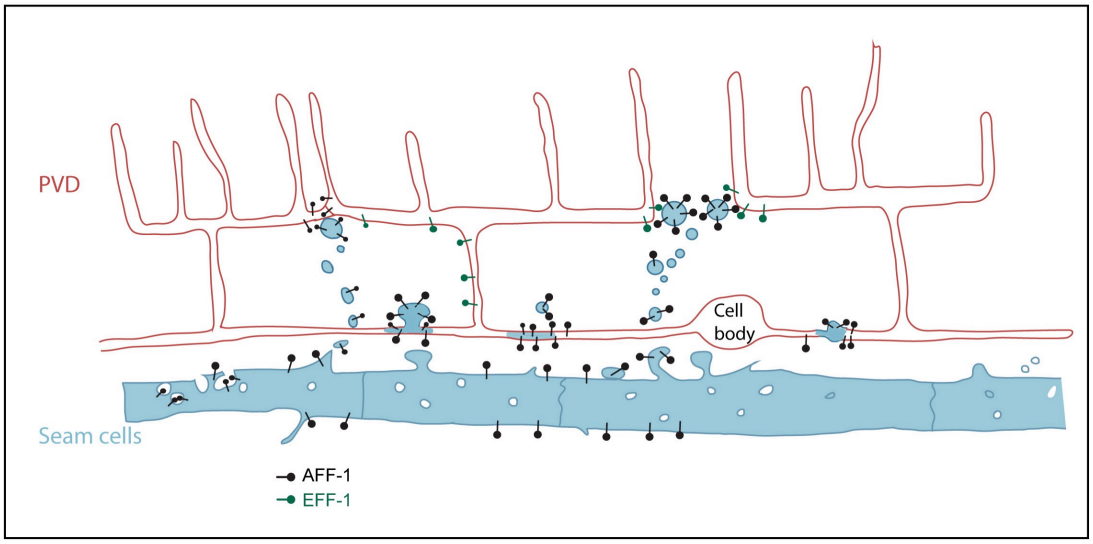

982
983
984 **Figure 5.**
985
986 **Model of AFF-1-mediated repair via extracellular vesicle-cell fusion**
987
988 PVD (red) is in close proximity to the epithelial seam cells (blue). AFF-1 (black pins)
989 is expressed in seam cells and additional tissues, but not in the PVD. Upon injury,
990 AFF-1-containing extracellular vesicles (EVs) are highly released from the seam
991 cells. Some of these EVs reach the PVD and promote fusion of severed dendrites.
992 EFF-1 (green pins) is expressed in the PVD but it does not act to fuse severed
993 dendrites on its own. Instead it may collaborate with AFF-1-EVs. We propose that
994 menorah-menorah fusion is mediated by AFF-1-EVs that merge with the structurally
995 compatible EFF-1 expressed in the PVD. EFF-1-coated pseudotyped viruses can fuse
996 with cells expressing AFF-1 on their surface and vice versa [64].
997

998 **Supplementary Figures**
999

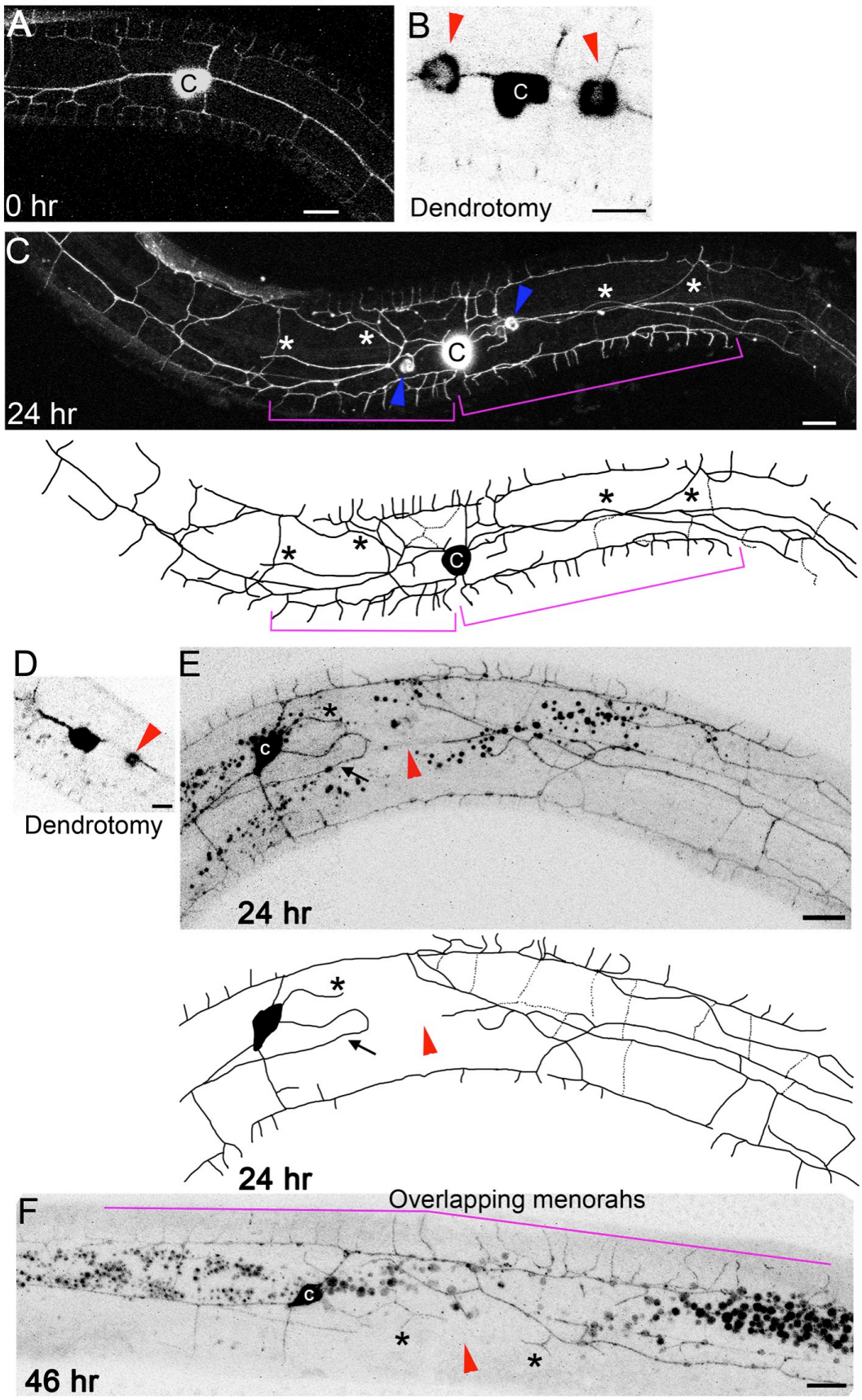

1000
1001

Figure 1-figure supplement 1.

Dendritic amputation induces hyper-branching, loss of self-avoidance and giant overlapping menorahs

(A) Wild-type animal before dendrotomy.

(B) Two laser-induced injuries of primary branches (red arrowheads, injury sites).

(C) Confocal projection and a schematic tracing of the same animal 24 hr post-surgery. Asterisks mark new sprouting from proximal and distal branches. Pink brackets, giant menorahs. Blue arrowheads, primary branch fusion.

(D) A different wild-type animal injured (red arrowhead) at the early L4 stage, recovered and analyzed 24 **(E)** and 46 hr **(F)** post-surgery. Black arrow, retrograde branch. The degenerating branches are represented as dotted lines in the schematic tracing. Scale bars represent 5 µm **(D)** and 10 µm **(A-C, E-F).**

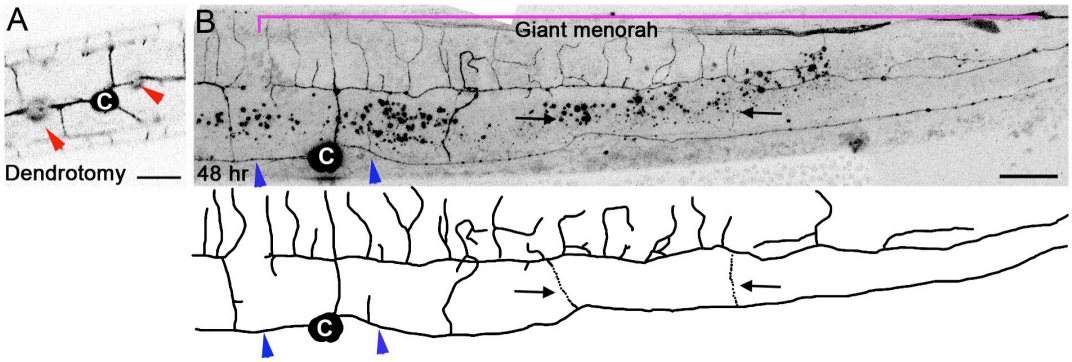

Figure 2- figure supplement 1.

Menorah fusion and 2ry stem pruning are part of the regeneration process of the PVDs following dendrotomy

(A) Dendrotomy of an L4 wild-type animal. Red arrowheads point to sites of laser surgery.

(B) Analysis 48 hr post-surgery. Giant menorah can be seen (pink bracket); arrows (and dotted lines in the schematic tracing) point to secondary branches undergoing trimming. Blue arrowheads mark primary branch fusion at the sites of dendrotomy. Scale bars represent 10 µm.

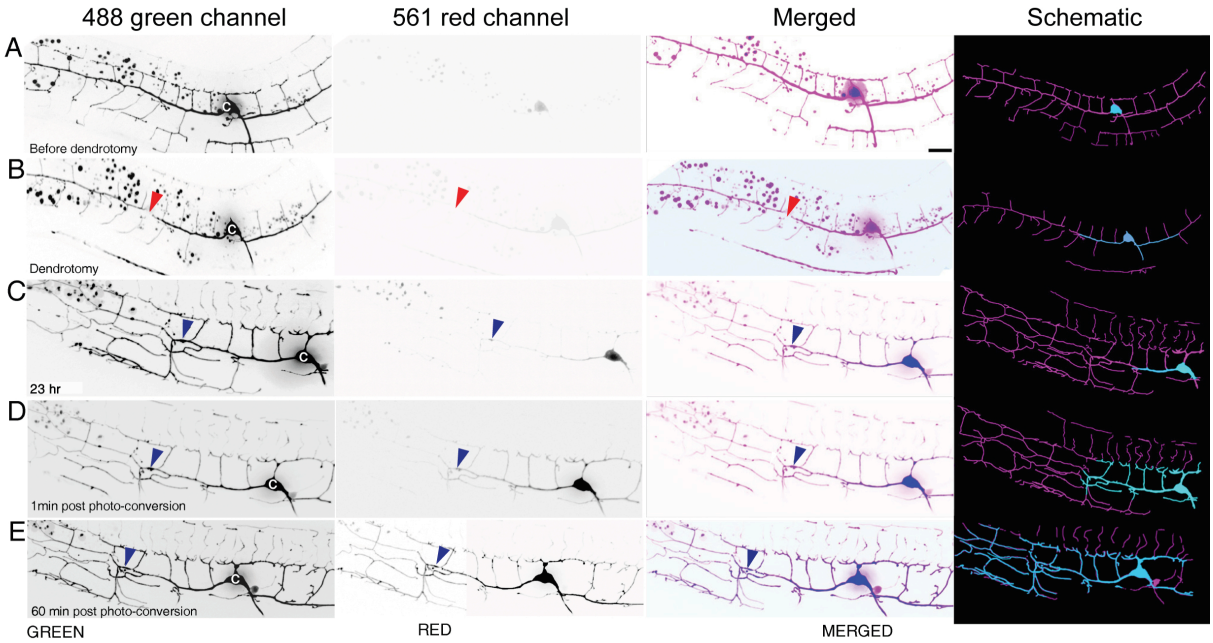

Figure 2-figure supplement 2.

PVD dendrite reconnection confirmed by Kaede photoconversion

A PVD primary dendrite of *ser-2prom3::Kaede* expressing animals was dendrotomized, the animal was recovered for 23 hr and the dendrite reconnection to its stump was assessed by Kaede photoconversion. The green Kaede form in the PVD cell body was irreversibly photo-converted to the red Kaede form using a 405nm laser with the Mosaic system and its spreading throughout the dendritic branches was followed 1 and 60 min post-photoconversion. Panels left to right are confocal reconstructions of a wild-type dendrotomized animal in the 488 green channel, 561 red channel, two channels merged view and a schematic representation of the merged view.

(A) Confocal reconstructions of the animal before dendrotomy, **(B)** immediately post dendrotomy, **(C)** 23 hr post-dendrotomy, **(D)** 1 min post Kaede photoconversion and **(E)** 60 min post Kaede photoconversion. Red Kaede form (cyan in merged and shematic representations), though diluted when spreading through the dendritic tree, can be observed beyond the reconnected site of injury in the distal part of the primary and higher ordered dendritic branches. Thus, Kaede photoconversion and diffusion beyond the injury site demonstrate fusion between the severed primary dendrite. In animals where reconnection failed photoconverted Kaede did not spread beyond the injury site (data not shown).
c, PVD cell body; red arrowhead, site of injury; blue arrowhead, site of primary branch fusion. In the merged and schematic columns: pink, green Kaede; cyan, photoconverted red Kaede.

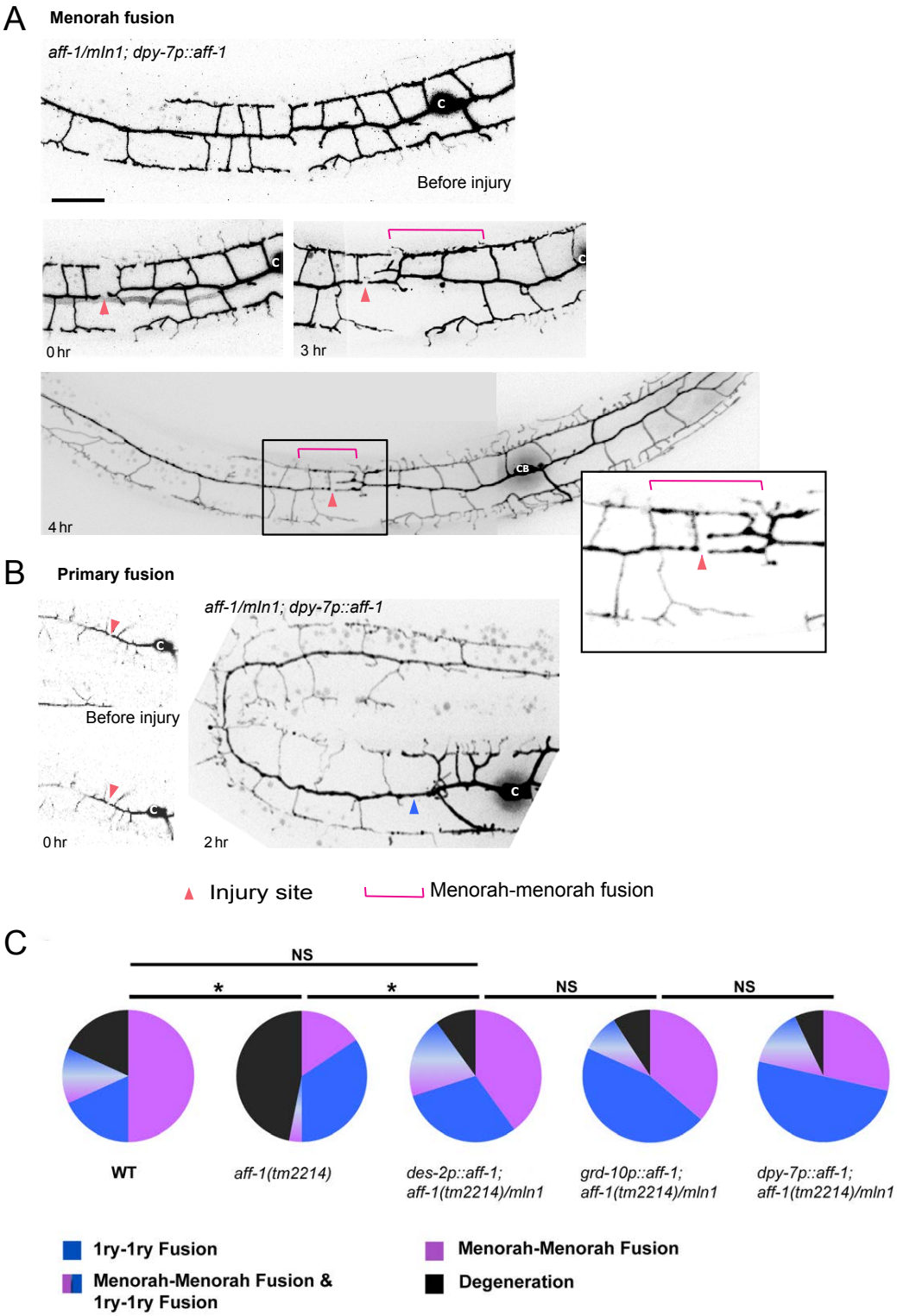

Figure 3-figure supplement 1.

Ectopic expression of hypodermal AFF-1 improves PVD regeneration in heterozygous animals

1077
1078 **(A)** Regeneration by menorah-menorah fusion following PVD nanosurgery in *C.*
1079 *elegans aff-1(tm2214)/mln1; dpy-7p::aff-1* animals. PVD is shown before and after
1080 nanosurgery (T=0, 3, and 4 hr). PVD reconnection occurred through fused menorahs
1081 (pink bracket) and primary fusion did not occur (red arrowhead).
1082
1083 **(B)** Dendrite regeneration following PVD primary branch nanosurgery in *C. elegans*
1084 *aff-1(tm2214)/mln1; dpy-7p::aff-1* animals. PVD is shown before and after
1085 nanosurgery (T=0 and 2 hr). PVD reconnection occurred through primary fusion (blue
1086 arrowhead).
1087
1088 **(C)** Animals showing different PVD post injury consequences displayed in color
1089 coded pie graphs as Magenta- Menorah-Menorah fusion, Blue- primary-primary
1090 fusion, Magenta and Blue- Menorah-Menorah fusion and primary-primary fusion,
1091 Black-degeneration. Wild type n=22; *aff-1(tm2214)* n=32; *aff-1/mln1; des-2p::AFF-1*
1092 n=10, *aff-1(tm2214) /mln1; grd-10p::aff-1* n=11, *aff-1(tm2214)/mln1; dpy-7p::aff*-1
1093 n=14. *P<0.05. P values for wild type and heterozygous genotypes are not significant
1094 (NS). Statistics was calculated using the Freeman-Halton extension of the Fisher exact
1095 probability test for a two-rows by four-columns contingency table,
1096 http://vassarstats.net/fisher2x4.html.
1097
1098 Dendrotomy site, red arrowhead; fused Menorah, pink bracket; primary fusion, blue
1099 arrowhead. Scale bars represent 20 µm.
1100

1101 **Supplemental movies legends**

1102

1103 **Movie 1. PVD dendrites touch and fuse following dendrotomy**

1104 Time lapse recording of an L4 wild-type animal just after injury. The z series images

1105 were recorded every 6 min, marker is *F49H12.4::GFP.* Arrows mark areas of fusing

1106 menorah tertiary branches. C marks PVD cell body.

1107 **Movie 2. A pseudo-colored presentation of depth information for Movie 1**

1108 Scale bar for the position in the z axis is shown at the bottom. The movie was

1109 obtained using the Zeiss LSM image browser DepthCod function.

1110 **Movie 3. Degeneration of the distal fragment following dendrotomy**

1111 Time lapse recording of a wild-type L4 animal after a two-photon injury. Posterior

1112 PVCR and PVCL are also marked with the *DES-2::GFP* marker and can be seen at

1113 the upper right corner. See **Figure 1G**.

1114 **Movie 4. Fusion and pruning during the PVD regeneration process**

1115 Intensity-values view of a time-lapse recording of an early L4 animal. Marker is

1116 *F49H12.4::GFP.* Menorahs from proximal and distal ends meet and fuse, bypassing

1117 the break induced by the two-photon injury. At the injury site growth and pruning of

1118 dendrites can be seen. Intensity scale bar is in **Figure 2D**.

1119 **Movie 5. AFF-1::GFP expression in PVD intact animals**

1120 Time lapse recording of *AFF-1::GFP* (cyan) expression inside and outside the seam

1121 cells (sc), and in the vulva (V) of an intact L4 animal shown in a two channels merged

1122 image. The z series images were recorded every 10 sec, PVD marker is

1123 *F49H12.4p::mCherry* (magenta). Arrows mark AFF-1 vesicles. See **Figure 4B**. The

1124 trajectory of vesicle 1 is shown in **Figure 4E**. Gut marks autofluorescent gut granules,

1125 easily distinguishable from AFF-1 vesicles in size, shape, and appearance in both
1126 channels.

1127 **Movie 6. AFF-1::GFP expression in PVD intact animals (zoom in of movie 5)**

1128 A magnification of a single *AFF-1::GFP* vesicle near the seam cells, ("vesicle 1").

1129 **Movie 7. AFF-1::GFP expression in PVD primary branch of injured animals**

1130 Time lapse recording of *AFF-1::GFP* expression (cyan) inside and outside the seam
1131 cells (sc), in the anchor cell (AC) and in the vulva (V) of a reconnected PVD L4
1132 animal after a two-photon injury anterior to PVD cell body. T=0 is 75 min after
1133 injury. The z series images were recorded every 20 sec, PVD marker is
1134 *F49H12.4p::mCherry* (magenta). Arrows point to vesicles containing AFF-1::GFP.

1135 **Movie 8. Magnification of Movie 7.**

1136 Magnification of an area with multiple vesicles, two are labeled (2,3). See **Figure 4**
1137 **D-E.**

1138 **Movie 9. AFF-1::GFP expression in PVD intact animal**

1139 Time lapse recording of *AFF-1::GFP* (cyan) expression inside and outside the seam
1140 cells (SC) of an intact L4 animal shown in a two channels merged image. The z series
1141 images were recorded every 10 sec, PVD marker is *F49H12.4p::mCherry* (magenta).
1142 Arrows mark AFF-1 vesicles.

1143 **Movies 10 and 11. AFF-1::GFP expression in a degraded PVD primary branch**
1144 **of injured animals** Time lapse recording of *AFF-1::GFP* expression (cyan) inside
1145 and outside the seam cells (sc) of a reconnected PVD L4 animal after a two-photon
1146 injury anterior to PVD cell body, red arrowhead is the site of injury. T=0 is 75 min
1147 (movie10) and 150 min (movie 11) after injury. The z series images were recorded
1148 every 2 sec, PVD marker is *F49H12.4p::mCherry* (magenta). Arrows point to vesicles
1149 containing AFF-1::GFP.